Supporting information

In vivo Selection for Formate Dehydrogenases with High Efficiency and Specificity towards $NADP^+$

Liliana Calzadiaz-Ramirez [1‡], Carla Calvó-Tusell [2‡], Gabriele M. M. Stoffel [3‡], Steffen N. Lindner [1], Sílvia Osuna [2,4], Tobias J. Erb [3,5], Marc Garcia-Borràs [2*], Arren Bar-Even [1*], Carlos G. Acevedo-Rocha [6*]

[1] Max Planck Institute of Molecular Plant Physiology, Am Mühlenberg 1, D-14476 Potsdam-Golm, Germany

[2] Institut de Química Computacional i Catàlisi and Departament de Química, Universitat de Girona, Carrer Maria Aurèlia Capmany 69, Girona 17003, Catalonia, Spain

[3] Max Planck Institute of Terrestrial Microbiology, Karl-von-Frisch-Str. 10, D-35043 Marburg, Germany

[4] ICREA, Pg. Lluís Companys 23, 08010 Barcelona, Spain

[5] LOEWE Research Center for Synthetic Microbiology (SYNMIKRO), Karl-von-Frisch-Str. 16, D-35043 Marburg, Germany

[6] Biosyntia ApS, 2100 Copenhagen, Denmark

‡ These authors contributed equally to this study.

* Corresponding authors: marcgbq@gmail.com (MGB), Bar-Even@mpimp-golm.mpg.de (ABE), car@biosyntia.com (CGAR)

Table of contents

1. Supporting results

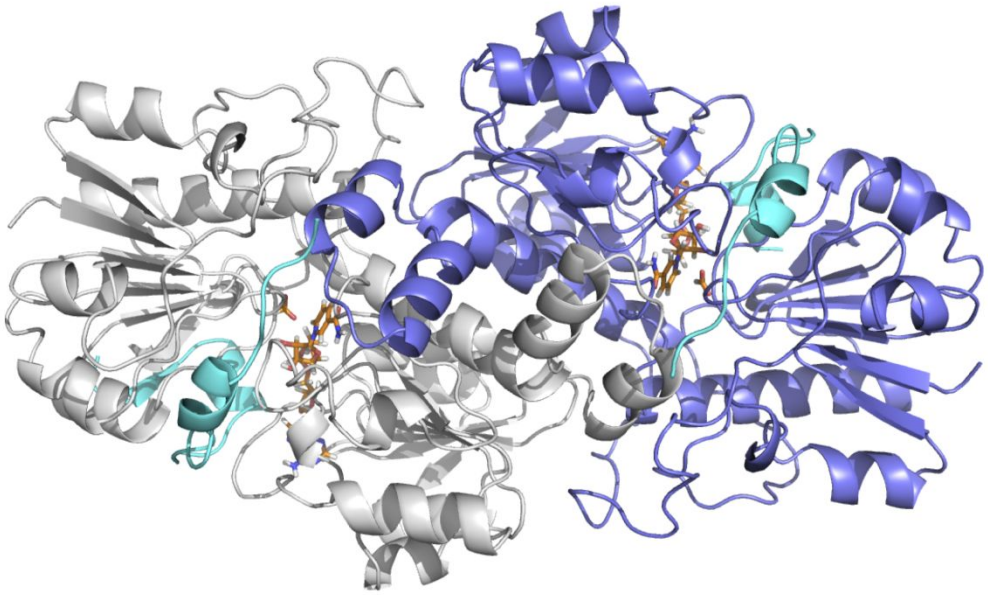

Figure S1. Overview of PseFDH enzyme.

The enzyme is a homodimeric complex formed by two non-covalently bound subunits (one subunit shown in grey and the other in purple). The X-Ray structure used as starting point for our MD simulations is based on PDBs 2GO1 [1] for the *apo* state and 2GUG [2] for the *holo* state. In these X-Ray structures, the cofactor NAD^+ and the important loop found in a region near cofactor binding (residues 375-400 depicted in cyan), were unsolved. This loop was reconstructed based on FDH X-ray structure PDB: 2NAD [3] (see computational details).

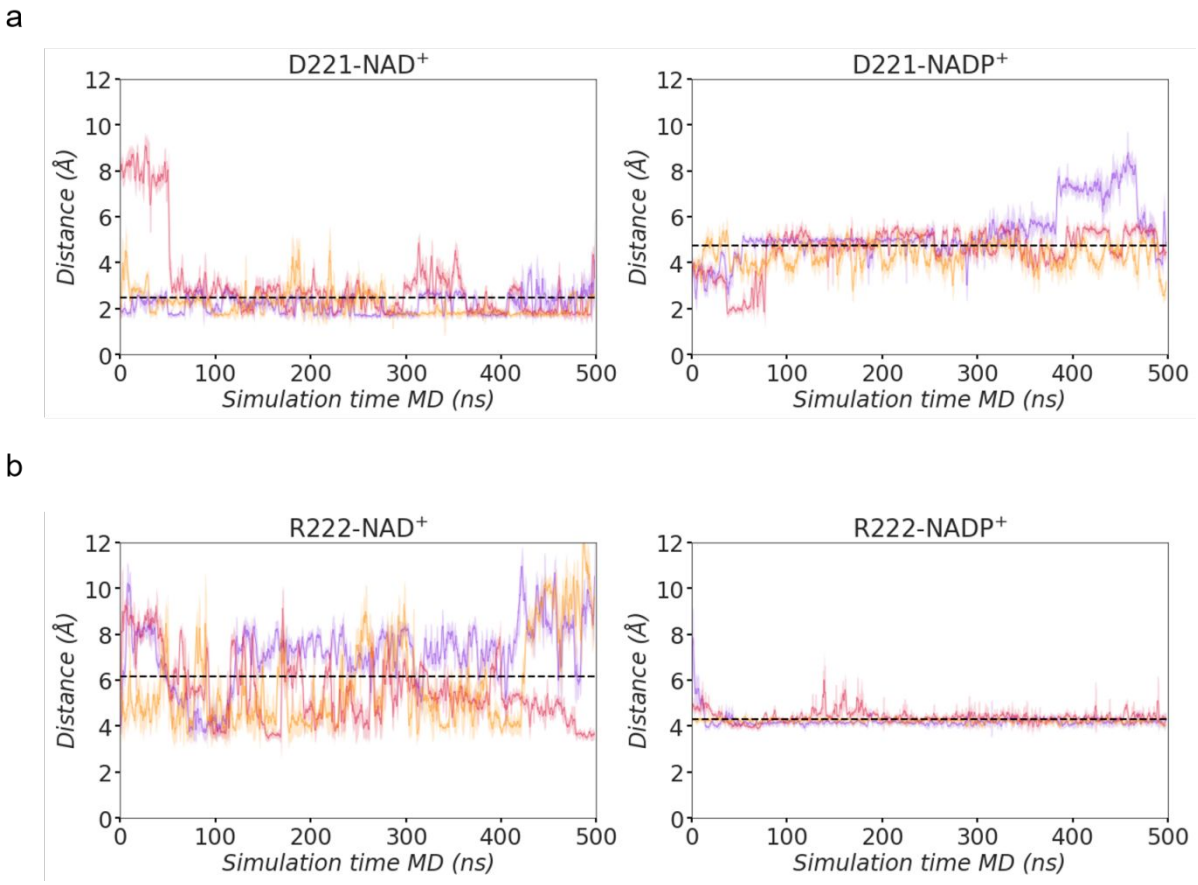

Figure S2. Comparison of the active site conformational dynamics of WT PseFDH in the presence of NAD^+ or $NADP^+$ cofactor and formate.

a) Plot of the distance between the carbon of the carboxylate group of D221 and 2'-OH group of NAD^+ (left) and the distance between the carbon of the carboxylate group of D221 and $NADP^+$ 2-' phosphate group (right) along 3 representative 500 ns replicas of MD simulations (shown in red, orange, and purple) for both WT-NAD^+ and WT-$NADP^+$ systems. Average distances from all replicas of 2.5 ± 1.2 Å and 4.7 ± 1.0 Å, respectively, are also shown with a dashed black line; and b) Plot of the distance between the carbon of the guanidinium group of R222 and 2'-OH group of NAD^+ (left) and the distance between the carbon of the guanidinium group of R222 and $NADP^+$ 2-' phosphate group (right) along 3 representative 500 ns replicas of MD simulations for both WT-NAD^+ and WT-$NADP^+$ systems. Average distances (dashed black line) of 6.2 ± 1.9 Å and 4.3 ± 0.4 Å, respectively, are also shown. All distances are represented in Å.

Purpose	Residue	Degenerate codon	AA alphabet
Cofactor-specificity	D221	RNC	ADGINSTV
	R222	CNA	LPQR
	H223	MVC	HNPRST
Activity recovery	Medium priority	Site-saturation mutagenesis	
	H258		
	E260		
	T261		
	S380		
	Low priority		
	H379		

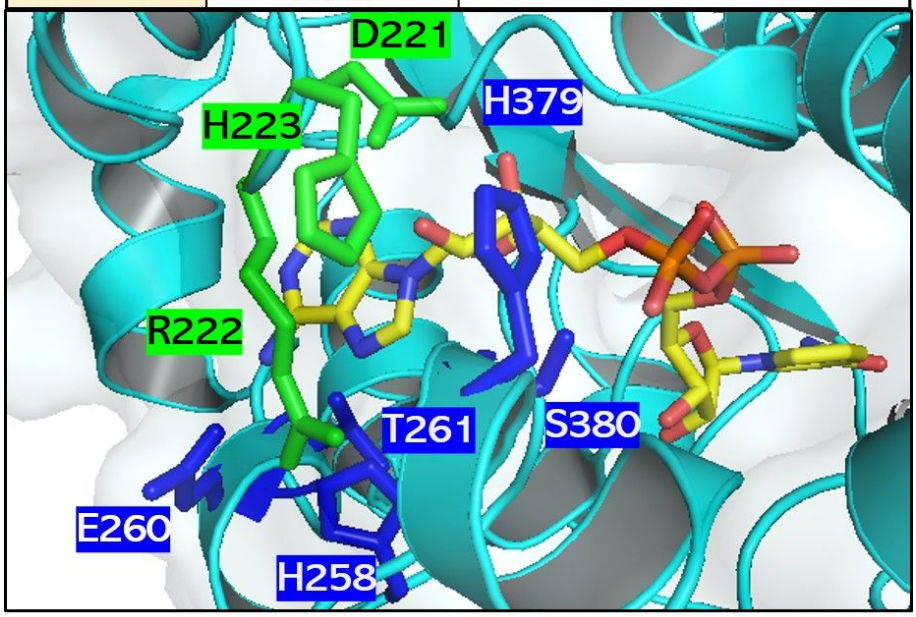

Figure S3. CRS-SALAD results.

Left: The by CRS-SALD server predicted mutagenesis of 3 active site residues (D221, R222 and H223) based on a library of 192 variants (8 x 4 x 6), followed by mutagenesis at 5 other residues to recover activity [4]. Right: The 8 residues were mapped on the PseFDH monomer highlighting the residues suggested by mutagenesis for switching cofactor specificity (green) and for recovering activity (blue) The carbon (yellow), nitrogen (blue) and oxygen (red) atoms of the cofactor are shown in stick format. Picture generated with PyMol using PDB file 2NAD [3].

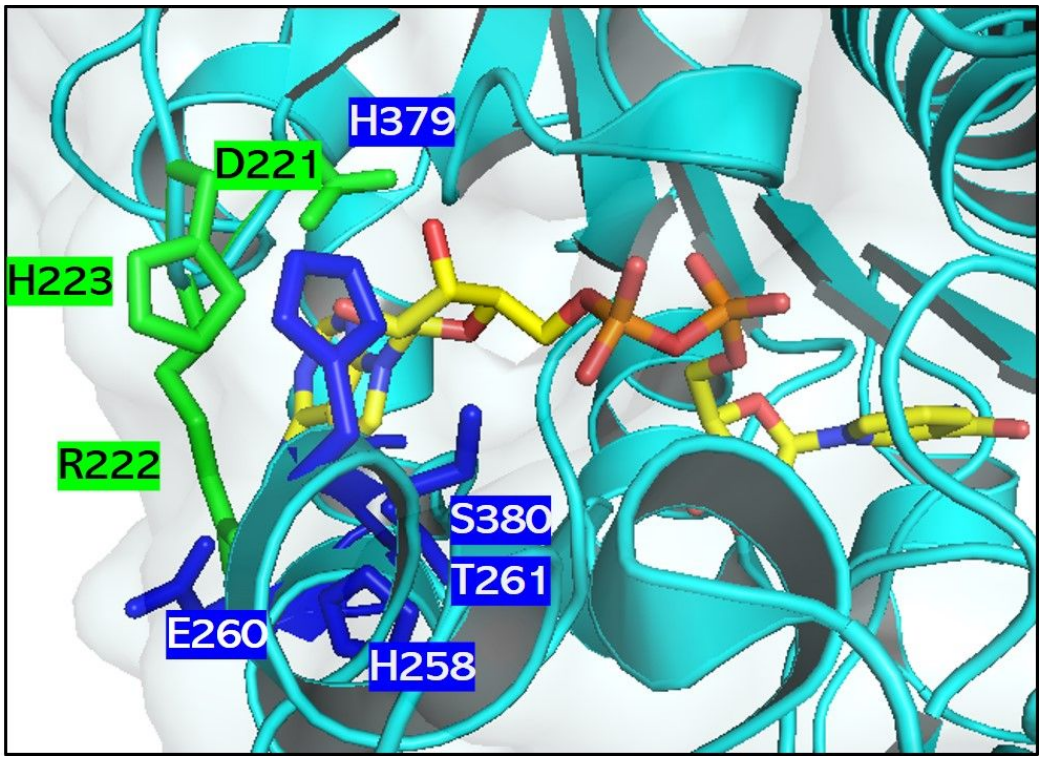

Figure S4. Grouping of activity-recovering residues.

Groups A (H379 and S380) and B (H258, E260, T261) residues (blue) were formed according to their proximity to selectivity residues D221, R222 and H223 (green). Residues D221 and H223 are closer to residue H379, which is adjacent to residue S380, whereas residue R222, which was not considered for mutagenesis in this study, lies among residues H258, E260 and T261. The carbon (yellow), nitrogen (blue) and oxygen (red) atoms of the cofactor are shown in stick format. Picture generated with PyMol using PDB file 2NAD [3].

I. SIMULTANEOUS RANDOMIZATION OF DIFFERENT POSITIONS USING DIFFERENT DEGENERATE CODONS			
Position 1	N	N	K
Position 2	N	N	K
Position 3	D	B	W
Position 4	N	N	K
Position 5	R	B	T

II. SET % COVERAGE and % WT background		95 0
Positions Randomized	**Codons**	**Colonies**
1		
1 + 2		
1 + 2 + 3		
1 + 2 + 3 + 4		
1 + 2 + 3 + 4 + 5	3538944	10601727

IMPORTANT: When different positions are randomized simultaneously it is important to select in each position a degeneracy that contains the correspondent wild-type aminoacid, otherwise the evaluation of the possible effects of the individual libraries would not be properly analyzed, as one of the positions is forced to be mutated.

The creation of libraries randomizing more than one codon using "**mutation forced**" **degeneracies** is as well interesting as the diversity generated differs strongly to the wild-type amino acid sequence.

Amino acids [AA] encoded in each position					
	1	**2**	**3**	**4**	**5**
Ala [A]	**2**	**2**	**2**	**2**	**1**
Arg [R]	**3**	**3**	**1**	**3**	0
Asn [N]	**1**	**1**	0	**1**	0
Asp [D]	**1**	**1**	0	**1**	0
Cys [C]	**1**	**1**	**1**	**1**	0
Gln [Q]	**1**	**1**	0	**1**	0
Glu [E]	**1**	**1**	0	**1**	0
Gly [G]	**2**	**2**	**2**	**2**	**1**
His [H]	**1**	**1**	0	**1**	0
Ile [I]	**1**	**1**	**2**	**1**	**1**
Leu [L]	**3**	**3**	**1**	**3**	0
Lys [K]	**1**	**1**	0	**1**	0
Met [M]	**1**	**1**	0	**1**	0
Phe [F]	**1**	**1**	**1**	**1**	0
Pro [P]	**2**	**2**	0	**2**	0
Ser [S]	**3**	**3**	**3**	**3**	**1**
Thr [T]	**2**	**2**	**2**	**2**	**1**
Trp [W]	**1**	**1**	0	**1**	0
Tyr [Y]	**1**	**1**	0	**1**	0
Val [V]	**2**	**2**	**2**	**2**	**1**
Stop	**1**	**1**	**1**	**1**	0
Codons	**32**	**32**	**18**	**32**	**6**
AA	**20**	**20**	**10**	**20**	**6**

Figure S5. CASTER results for PseFDH library.

This program allwos calculating the library sizes at both DNA and amino acid level for up to 5 residues as well as different library coverage percentages.

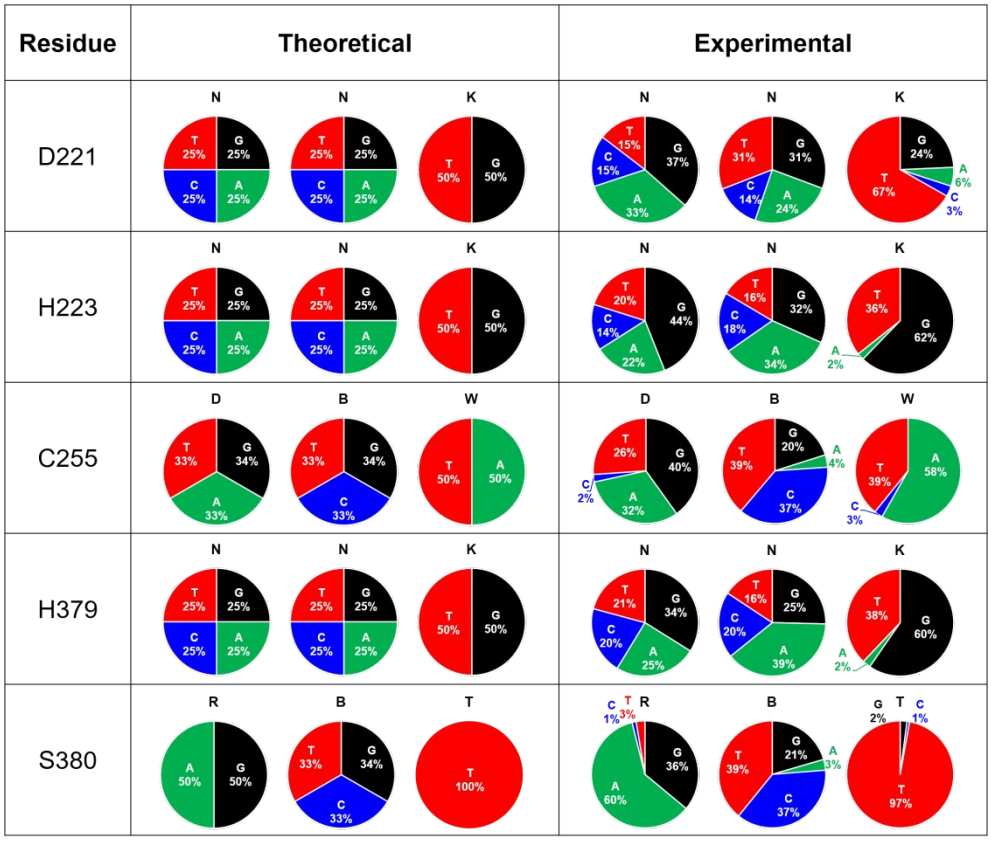

Figure S6. QQC of PseFDH library.

Pie charts representing the percentage of each base at each position of residues D221, H223, C255, H379 and S380.

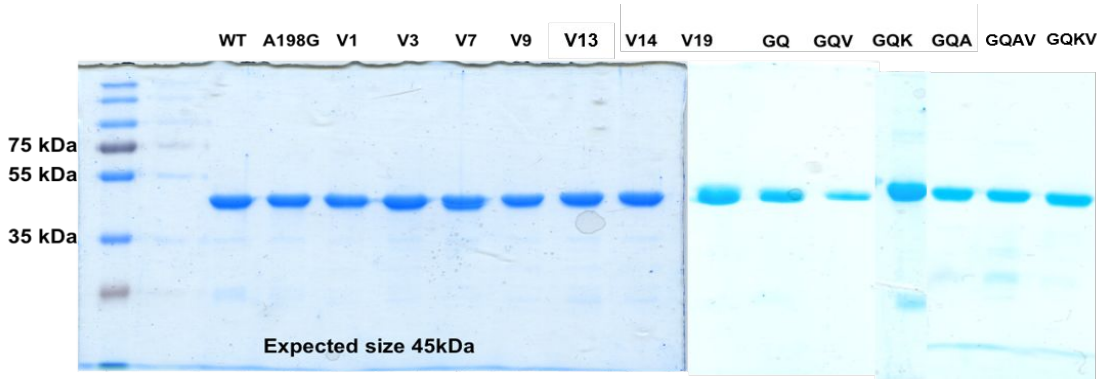

Figure S7. SDS-PAGE of purified PseFDH mutants.

About 3 mg of purified protein were loaded in each well of a 12.5% polyaacrylamide gel. Left: Protein bands for the WT and 7 variants isolated from the selection experiment. Right: Proteins bands for the deconvoluted mutants GQ (A198G/D221Q), GQV (A198G/D221Q/S380V), GQK (A198G/D221Q/H379K), GQA (A198G/D221Q/C255A), GQAV (A198G/D221Q/C255A/S380V) and GQKV (A198G/D221Q/H379K/S380V).

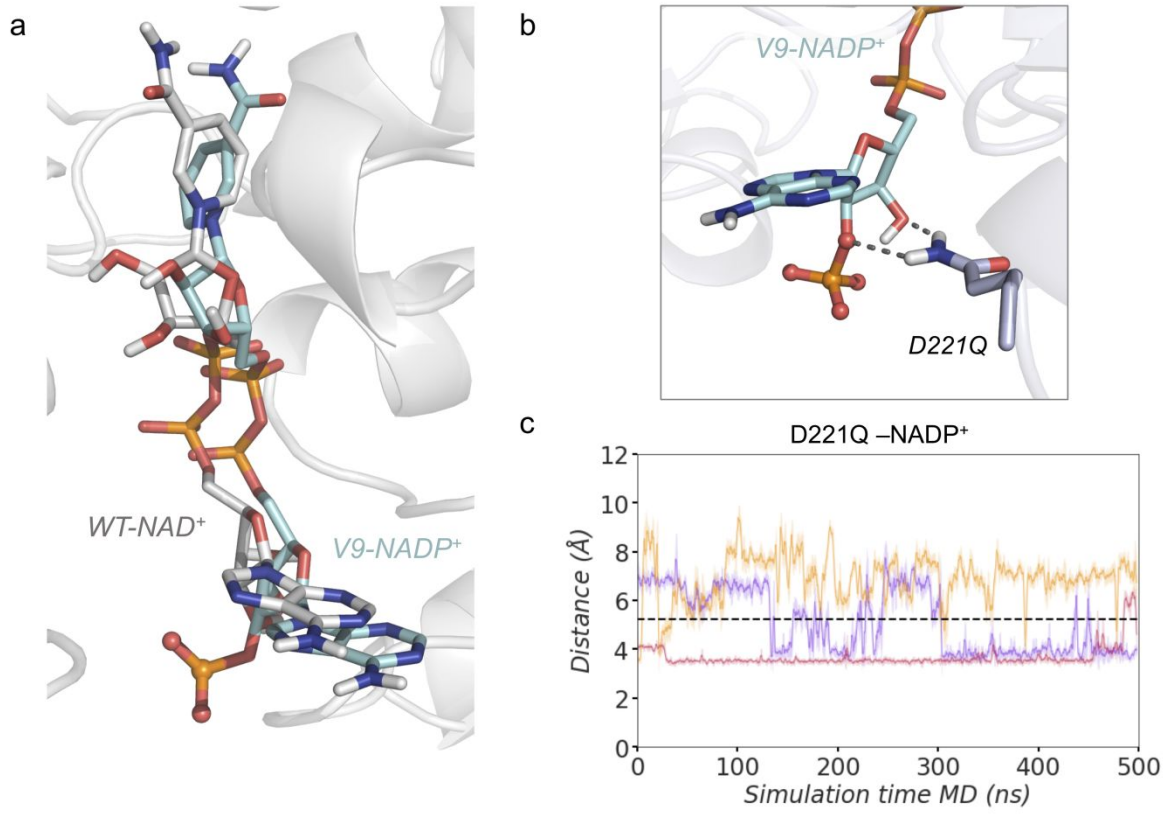

Figure S8. MD simulations analysis with focus on mutation D221Q.

a) Overlay of PseFDH WT-NAD$^+$ (grey) and variant V9-NADP$^+$ (cyan) representative conformations of the binding pocket. The figure shows that the adenine ring of both WT-NAD$^+$ and V9-NADP$^+$ are found in the same orientation. However, the nicotinamide ring of the V9-NADP$^+$ is rotated with respect to WT-NAD$^+$. The Root-Mean-Square-Deviation (RMSD) of the cofactor NADP$^+$ in the variant V9 with respect to the natural NAD$^+$ cofactor in the WT enzyme is 2.1 Å. b) Representative structure of the frequently observed hydrogen bonds established between D221Q and the 2'-phosphate and 3'-OH group of NADP$^+$. c) Plot of the distance of the hydrogen bond established between D221Q and the 2'-phosphate and 3'-OH group of NADP$^+$ along 3 replicas of 500 ns of MD simulations for the V9-NADP$^+$ (replicas are shown in purple, orange and red). Average distance from all replicas (dashed black line) of 5.2 ± 1.7 Å is also depicted. All distances are represented in Å.

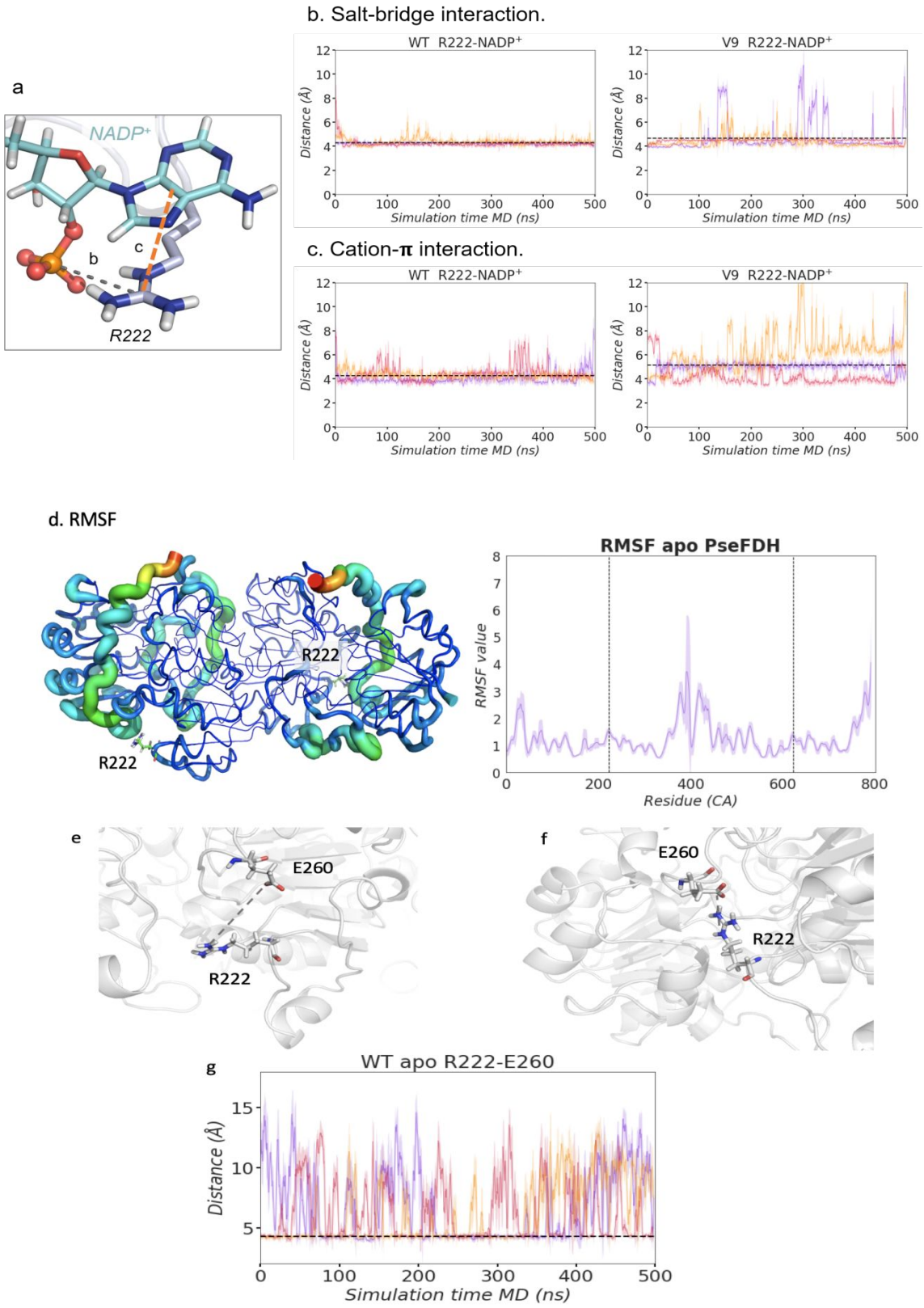

Figure S9. MD simulations analysis focused on residue R222 conformational dynamics and interactions.

a) Representative structure of V9-NADP⁺ binding pocket with the salt-bridge interaction between the guanidinium group of R222 and the 2'-phosphate group of NADP⁺ and the cation-π between the guanidinium group of R222 and the adenine group of NADP⁺ highlighted. b) Plot of the distance of the salt-bridge interaction between the carbon of the guanidinium group of R222 and the 2'-phosphate group of NADP⁺ along 3 replicas of 500 ns of MD simulations for the WT-NADP⁺ and the V9-NADP⁺ (red, orange and purple lines). Average distances (dashed black line) of 4.3 ± 0.4 Å and 4.4 ± 1.2 Å, respectively, are also included. c) Plot of the distance of the cation-π interaction between the guanidinium group of R222 and the center of mass of the adenine group of NADP⁺ along 3 replicas of 500 ns of MD simulations for the WT-NADP⁺ and the V9-NADP⁺. Average distances (dashed black line) of 4.3 ± 0.7 Å and 5.2 ± 1.4 Å, respectively, are also shown. d) Root-Mean-Square-Fluctuation (RMSF) analysis of alpha carbons of apo state PseFDH computed from 3 replicas of 500 ns of MD simulations. e) Solvent exposed conformation of R222 side chain in apo PseFDH explored along MD simulations. f) Interaction between R222 and E260 apo PseFDH observed in MD simulations. g) Plot of the distance between the carbon of the guanidinum group of R222 and the carbon of the carboxylic group of E260 along 3 replicas of 500 ns of MD simulations for the apo state of PseFDH enzyme. All distances are represented in Å.

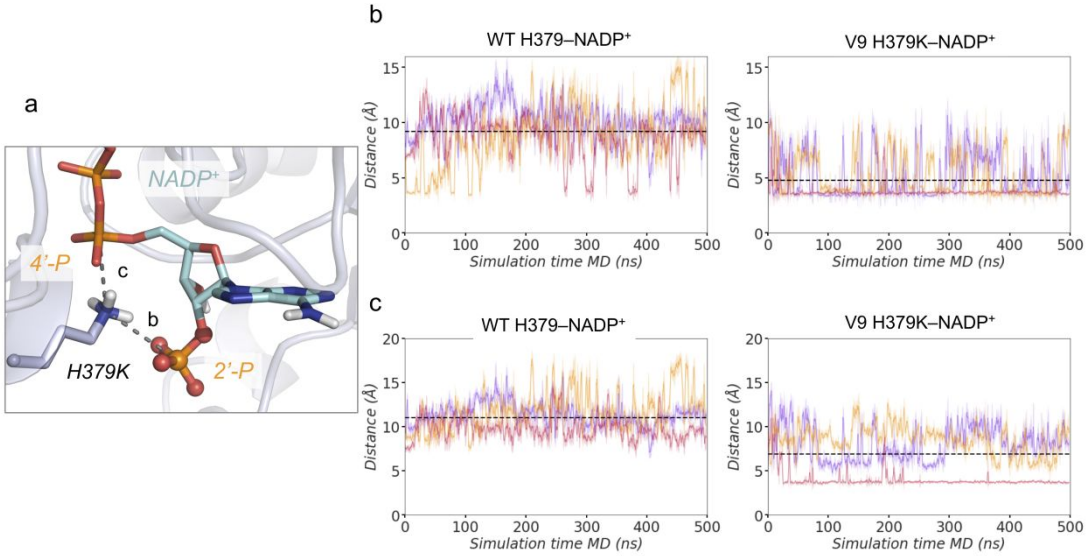

Figure S10. MD simulations analysis with focus on mutation H379K.

a) Representative structure of V9-NADP⁺ binding pocket with the salt-bridge interaction between the positively charged amino group of H379K and the 2'-phosphate group of NADP⁺ and the salt-bridge interaction between the positively charged amino group of H379K and the linker 4'-phosphate group of NADP⁺ highlighted. b) Plot of the distance between the ε-nitrogen of H379 and the 2'-phosphate group of NADP⁺ along 3 replicas of 500 ns of MD simulations (shown in red, orange and purple) for the WT-NADP⁺ (left) and plot of the distance of the salt-bridge interaction between the positively charged amino group of H379K and the 2'-phosphate group of NADP⁺ along 3 replicas of 500 ns of MD simulations for the V9-NADP⁺ (right). Average distances from all replicas (dashed black line) of 9.2±2.5 Å and 4.8±2.0 Å, respectively, are additionally included. c) Plot of the distance between the ε-nitrogen of H379 and the linker 4'-phosphate group of NADP⁺ along 3 replicas of 500 ns of MD simulations for the WT-NADP⁺ (left) and plot of the distance of the salt-bridge interaction between the positively charged amino group of H379K and the linker 4'-phosphate group of NADP⁺ along 3 replicas of 500 ns of MD simulations for the V9-NADP⁺ (right). Average distances (dashed black line) of 11.0±1.2 Å and 6.9±2.7 Å, respectively, are also shown. All distances are represented in Å.

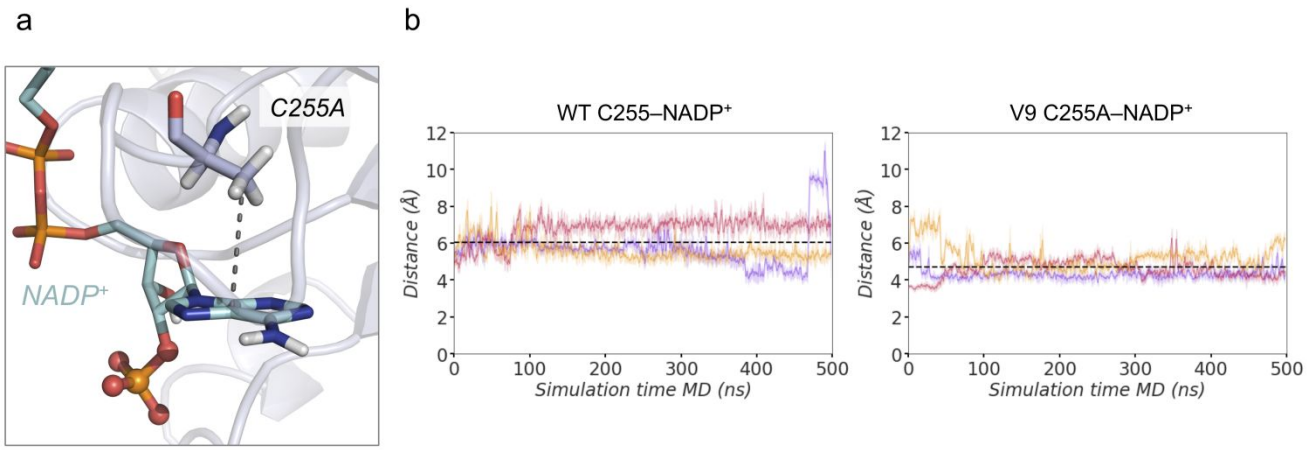

Figure S11. MD simulations analysis with focus on mutation C255A.

a) Representative structures of WT-NADP$^+$ (left) and V9-NADP$^+$ (right) binding pocket with the CH$\cdots\boldsymbol{\pi}$ interaction between the adenine ring of NADP$^+$ and the β-carbon of the side chain of C255 in the case of WT (left) and the β-carbon of the side chain of C255A in the case of V9 (right) highlighted. b) Plot of the distance between the center of mass (COM) of the NADP$^+$ adenine ring and the β-carbon of the side chain of C255 in the case of WT (left) and the β-carbon of the side chain of C255A in the case of V9 (right) along 3 replicas of 500 ns of MD simulations (shown in red, orange, and purple) for the WT-NADP$^+$ and the V9-NADP$^+$. Average distances from all replicas of 6.0±1.0 Å and 4.7±0.7 Å, respectively, are also shown with a dashed black line. All distances are represented in Å.

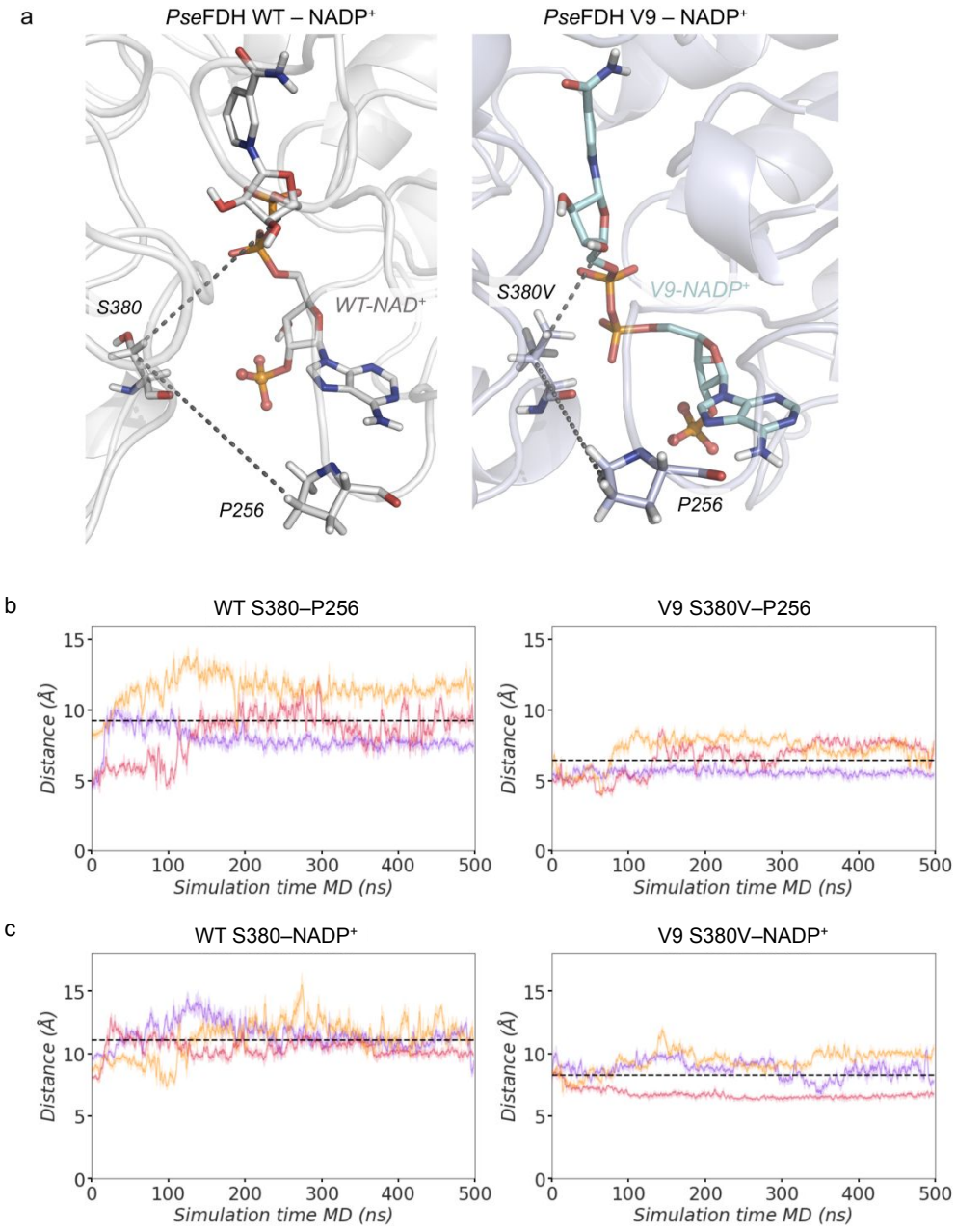

Figure S12. MD simulations analysis with focus on mutation S380V.

a) Representative structures of WT-NADP$^+$ (left) and V9-NADP$^+$ (right) binding pocket with the interactions between the β-carbon of the side chain of S380(WT)/V380(V9) and the β-carbon of the side chain of P256 and the interactions between the β-carbon of the side chain of S380(WT)/V380(V9) and the nicotinamide ribose group of NADP$^+$ highlighted. b) Plot of the distance between the β-carbon of the side chain of S380(WT)/V380(V9) and the β-carbon of the side chain of P256 along 3 replicas of 500 ns of MD simulations for the WT-NADP$^+$ and the V9-NADP$^+$. Average distances from all replicas (dashed black line) of 9.2±2.1 Å and 6.5±1.1 Å, respectively, are also included. c) Plot of the distance between the β-carbon of the side chain of S380(WT)/V380(V9) and the nicotinamide ribose group of NADP$^+$ along 3 replicas of 500 ns of MD simulations for the WT-NADP$^+$ and the V9-NADP$^+$. Average distances of 11.1±1.3 Å and 8.3±1.4 Å, respectively, are shown with a dashed black line. All distances are represented in Å.

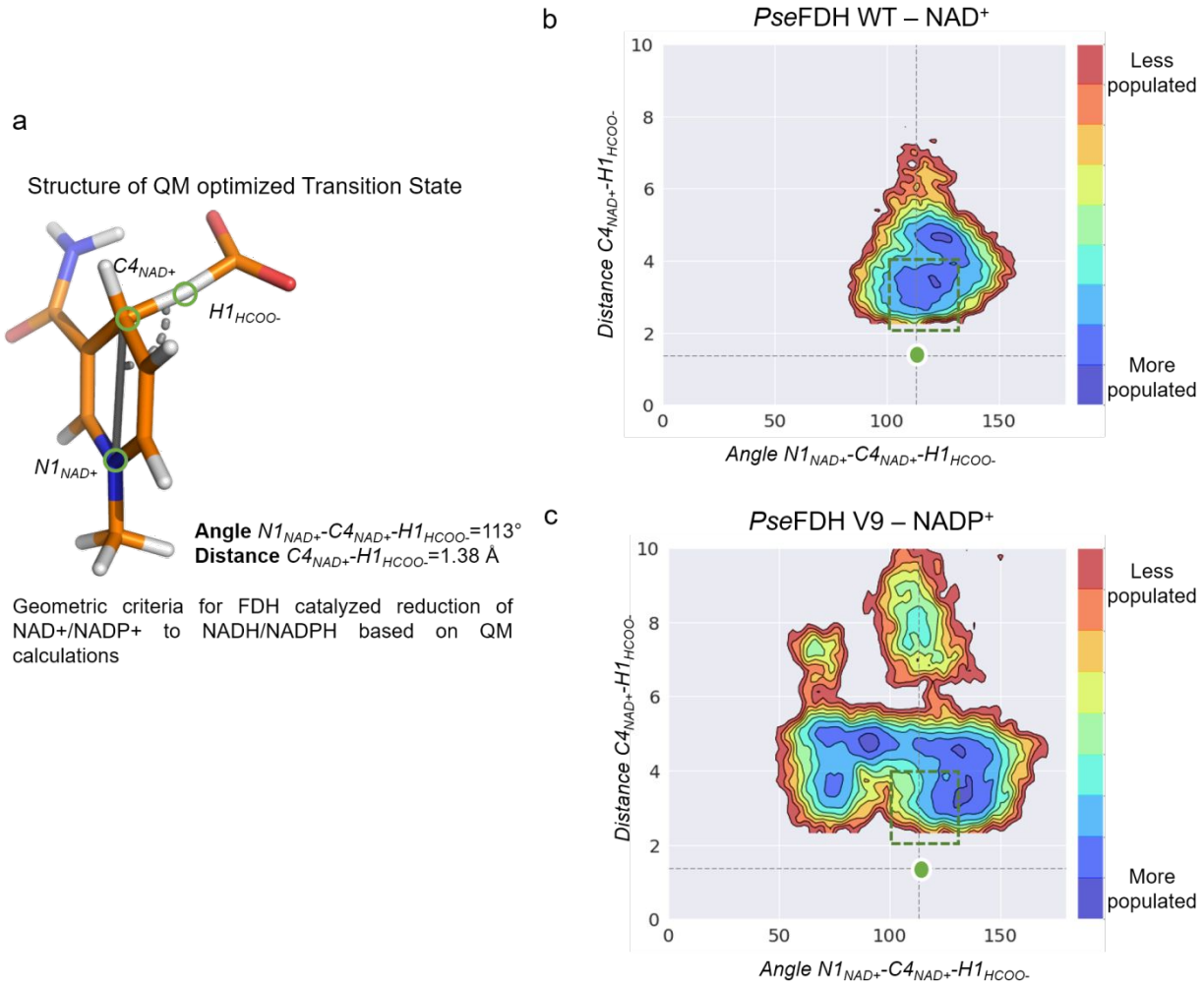

Figure S13. QM studies and conformational population analysis based on QM-derived geometric criteria.

a) Structure of the QM optimized Transition State for PseFDH catalyzed reduction of NAD^+/$NADP^+$ with the optimal angle and distance for hydride transfer reaction. A truncated computational model of the cofactor was used in the TS calculations (see computational details). b) Conformational population analysis based on the geometric criteria (hydride transfer distance versus angle) for PseFDH hydride transfer in the case of WT-NAD^+. c) Conformational population analysis based on the geometric criteria (hydride transfer distance versus angle) for PseFDH hydride transfer in the case of V9-$NADP^+$. The plots have been constructed using the angle $N1_{NAD+/NADP+}$-$C4_{NAD+/NADP+}$-$H1_{HCOO-}$ and the distance $C4_{NAD+/NADP+}$-$H1_{Hcoo-}$ sampled along 3 replicas of 500 ns MD simulations for WT-NAD^+ and V9-$NADP^+$. The catalytic distance (1.38 Å, represented by a horizontal dashed black line; value obtained from QM calculation) and the proper angle (*ca.* 113º, represented by a vertical dashed black line; value obtained from QM calculation) required for hydride transfer is represented by a green dot. The range of distances and angles considered as catalytically relevant in our MD simulations are those found within the green box (distances that range from 2 to 4 Å and angles from 100º to 130º).

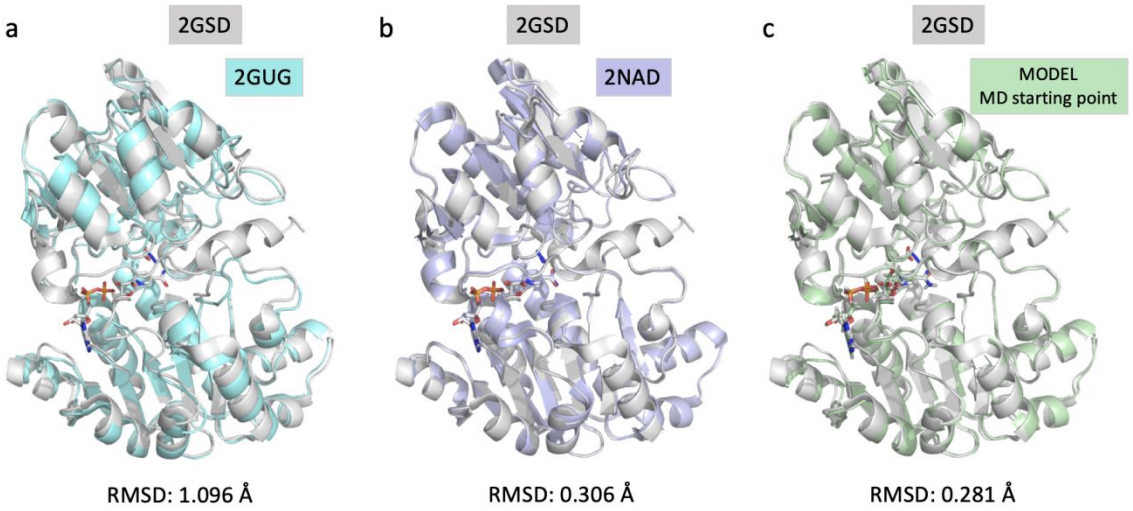

Figure S14. Comparison of the selected structures with the holo-MorFDH (PDB:2GSD).

Comparison of structures of PseFDH holo 2GUG (cyan), ternary complex 2NAD (purple) and the constructed model for the ternary complex (green) with the reference structure of holo MorFDH structure 2GSD (grey). Root-Mean-Square-Deviation (RMSD) values (in Å) considering all the atoms are depicted in the figure using the PDB 2GSD as a reference. Only one monomer is shown.

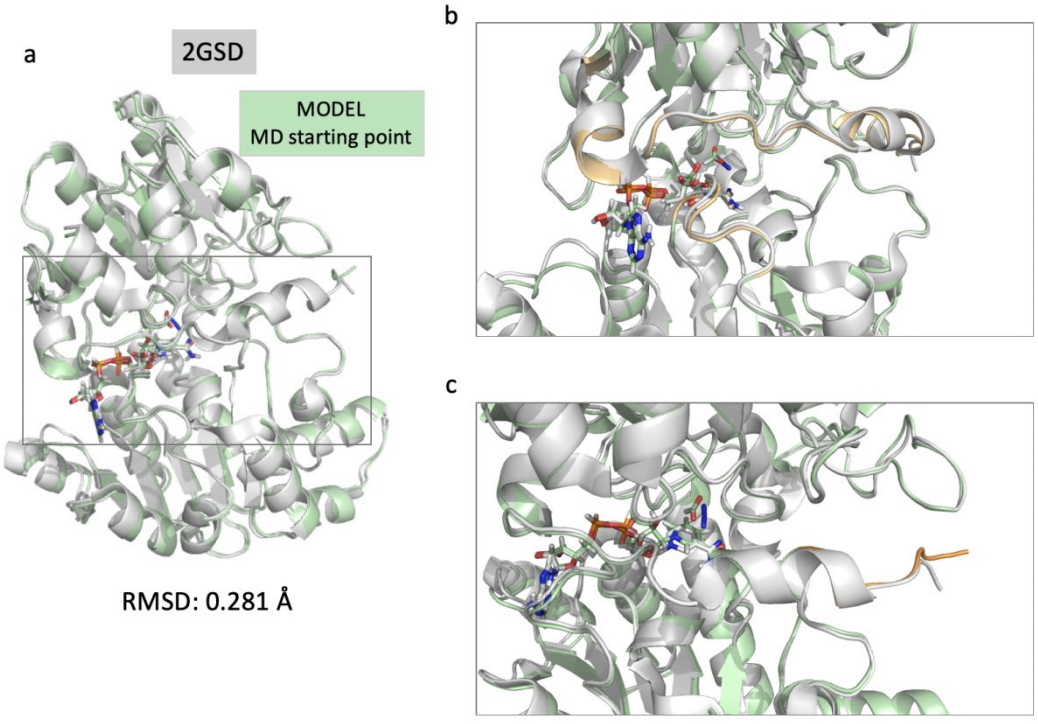

Figure S15. Comparison of structures of PseFDH holo 2GUG with the reference structure of holo MorFDH structure 2GSD.

a) Comparison of structure of the constructed model for the ternary complex (green) with the reference structure of holo MorFDH structure 2GSD (grey). b) Unsolved regions that were reconstructed with homology modelling tools are shown in orange. c) Residues 393-400 that were not present in the reference 2NAD structure were present in the final model used as starting point for MD simulations. The 7 extra residues are depicted in orange.

WT

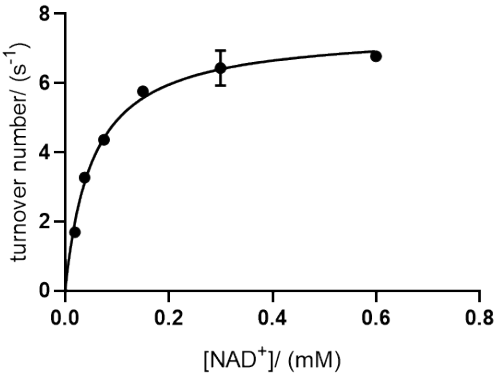
turnover number/ (s-1)
[NAD+]/ (mM)

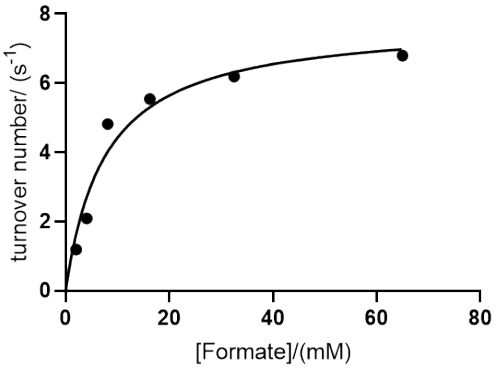
turnover number/ (s-1)
[Formate]/(mM)

V1

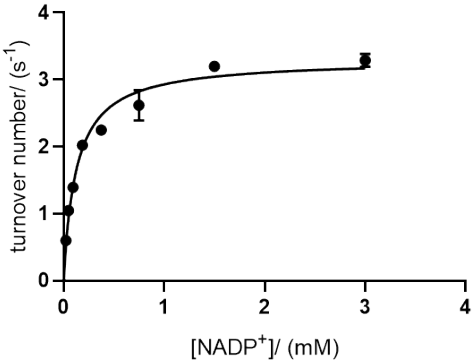
turnover number/ (s-1)
[NADP+]/ (mM)

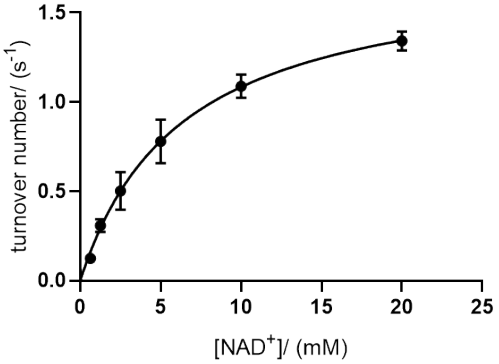
turnover number/ (s-1)
[NAD+]/ (mM)

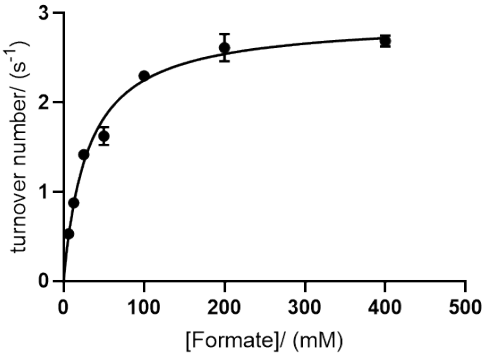
turnover number/ (s-1)
[Formate]/ (mM)

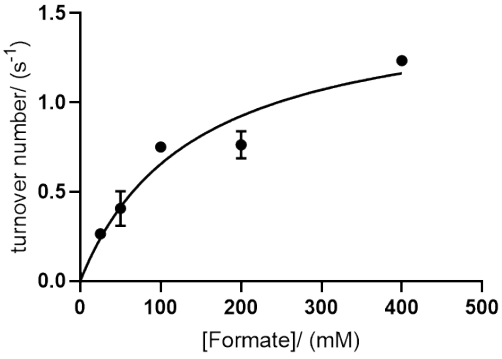
turnover number/ (s-1)
[Formate]/ (mM)

V3

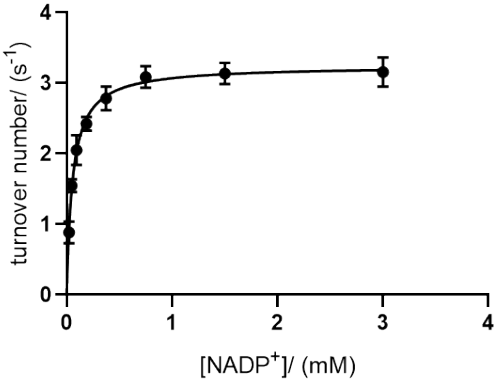
turnover number/ (s-1)
[NADP+]/ (mM)

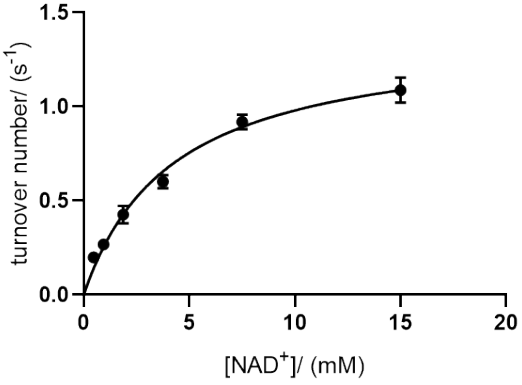
turnover number/ (s-1)
[NAD+]/ (mM)

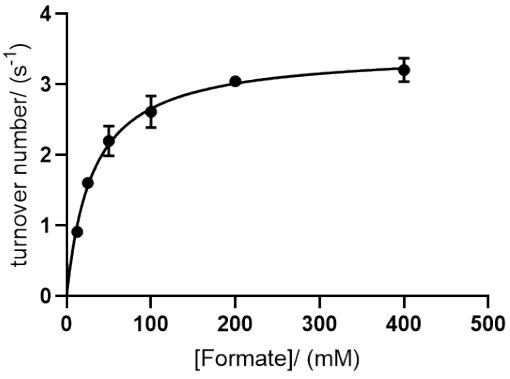
turnover number/ (s-1)
[Formate]/ (mM)

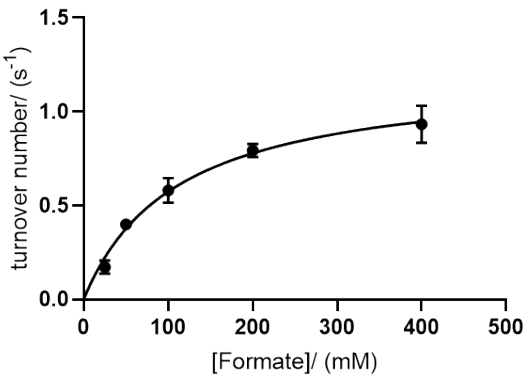
turnover number/ (s-1)
[Formate]/ (mM)

V7

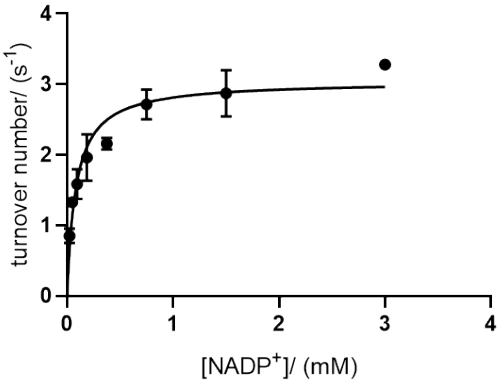
turnover number/ (s-1)
[NADP+]/ (mM)

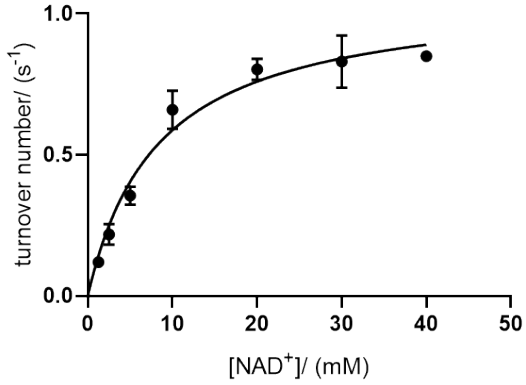
turnover number/ (s-1)
[NAD+]/ (mM)

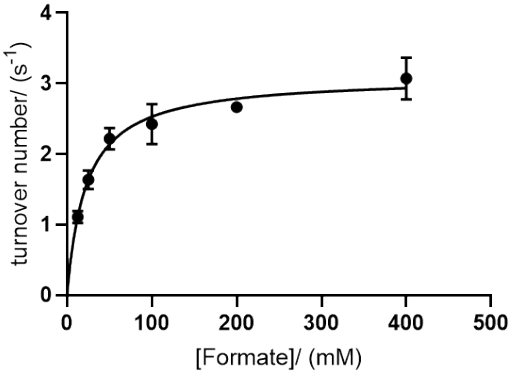
turnover number/ (s-1)
[Formate]/ (mM)

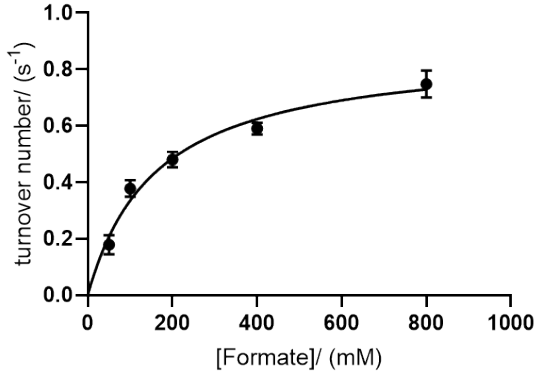
turnover number/ (s-1)
[Formate]/ (mM)

V9

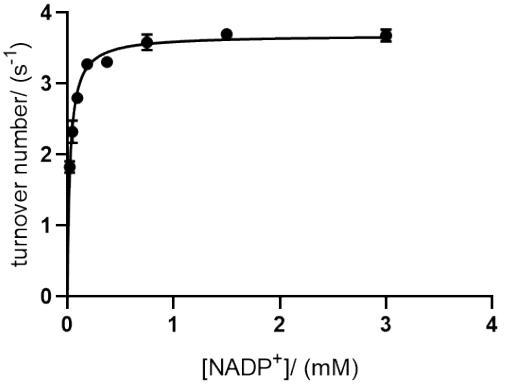
turnover number/ (s-1)
[NADP+]/ (mM)

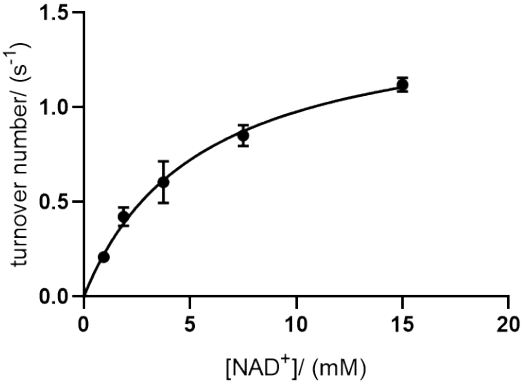
turnover number/ (s-1)
[NAD+]/ (mM)

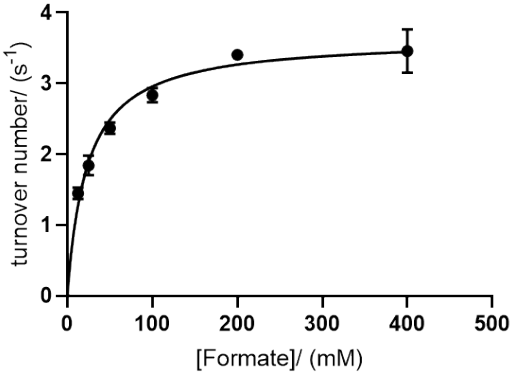
turnover number/ (s-1)
[Formate]/ (mM)

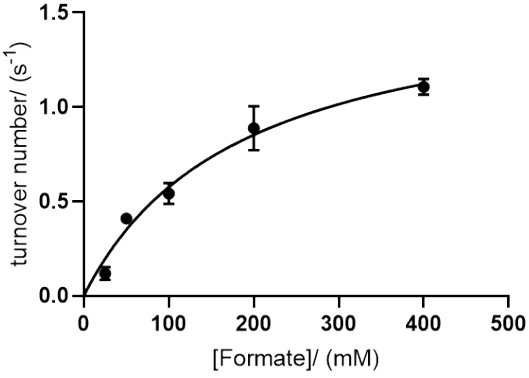
turnover number/ (s-1)
[Formate]/ (mM)

V13

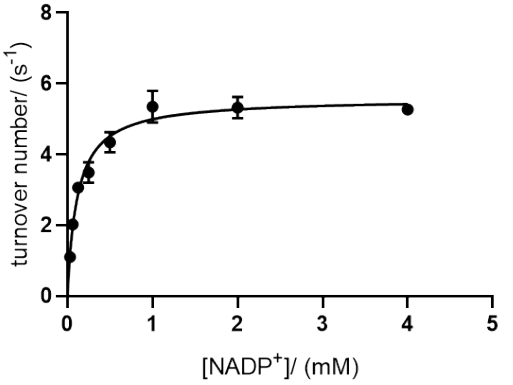
turnover number/ (s-1)
[NADP+]/ (mM)

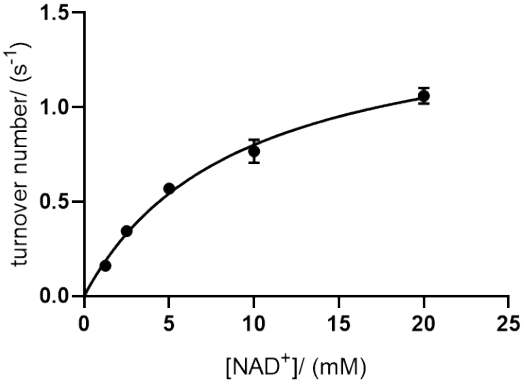
turnover number/ (s-1)
[NAD+]/ (mM)

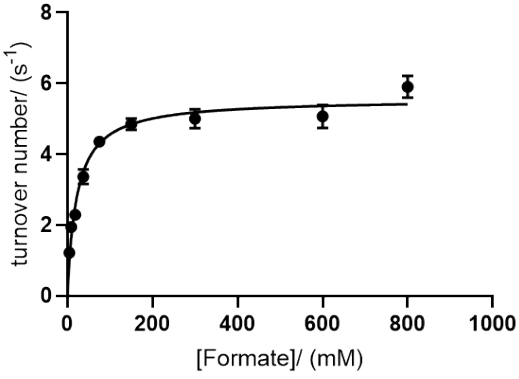
turnover number/ (s-1)
[Formate]/ (mM)

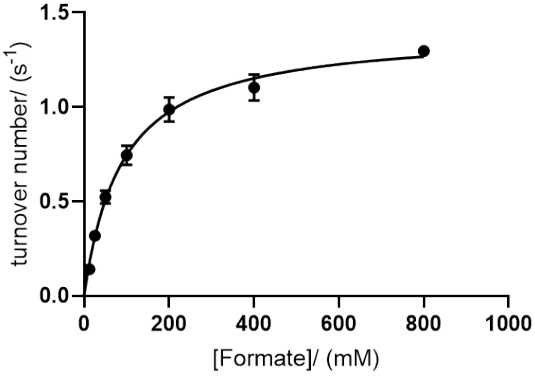
turnover number/ (s-1)
[Formate]/ (mM)

V14

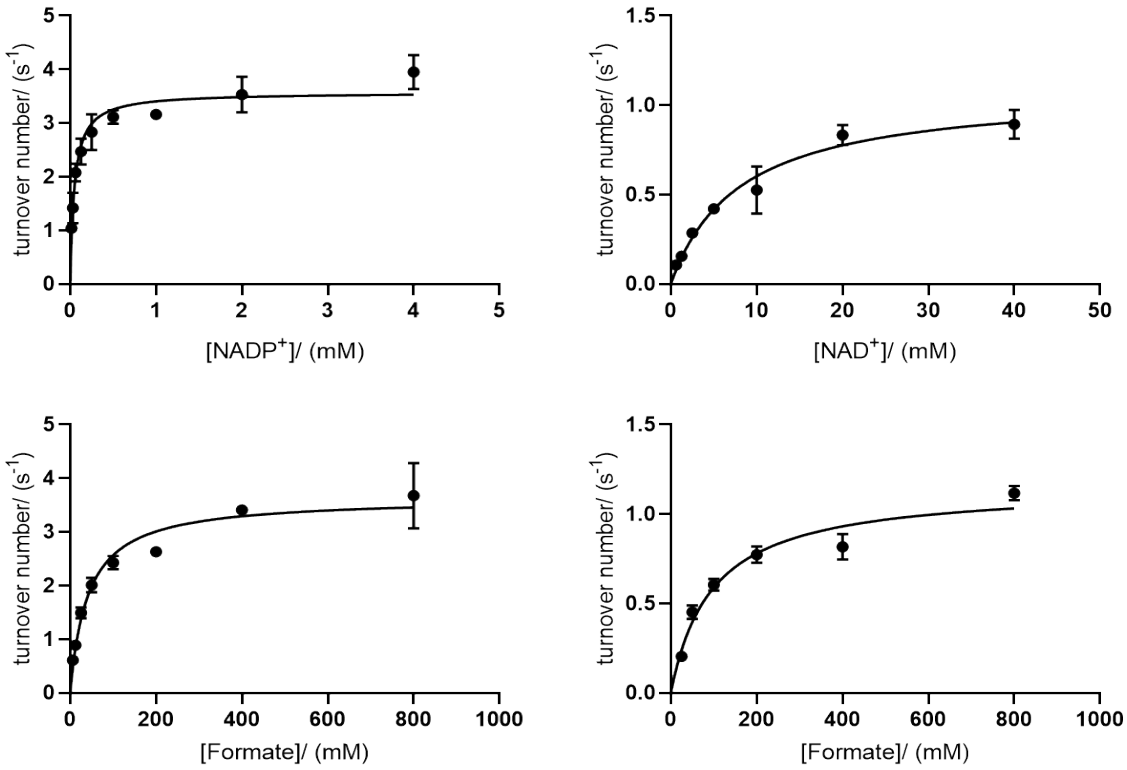

V19

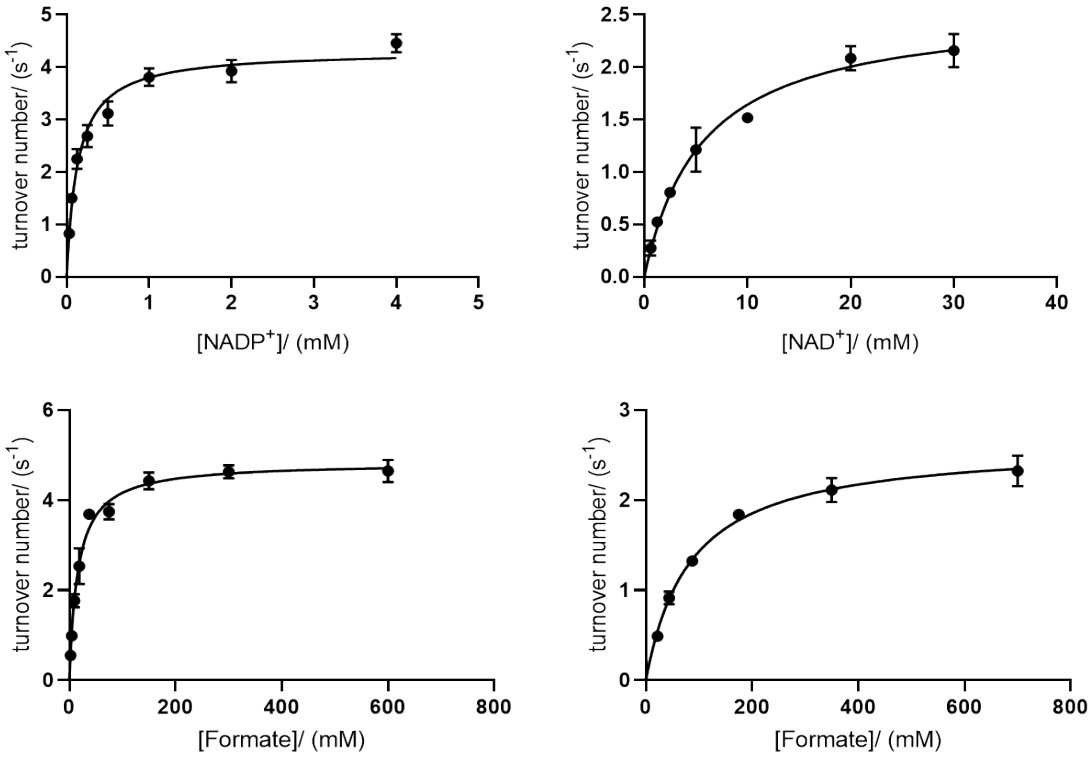

Figure S16. Michaelis Menten curves for selected PseFDH variants.

Variant G (A198G)

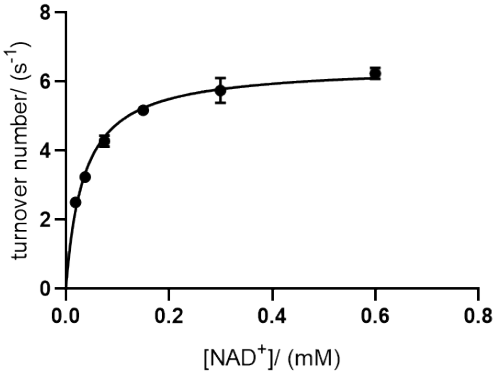

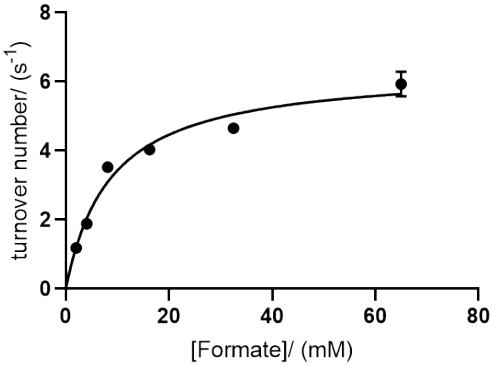

Variant GQ (A198G/D221Q)

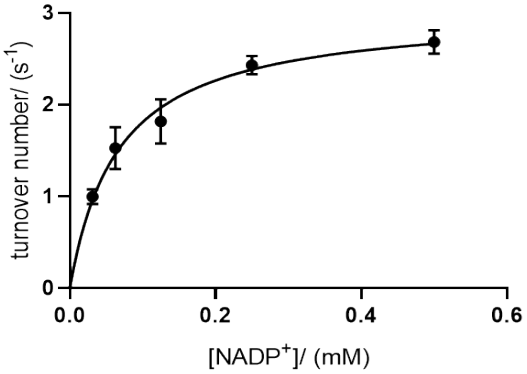

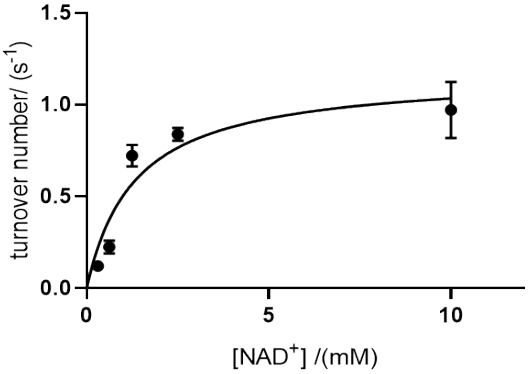

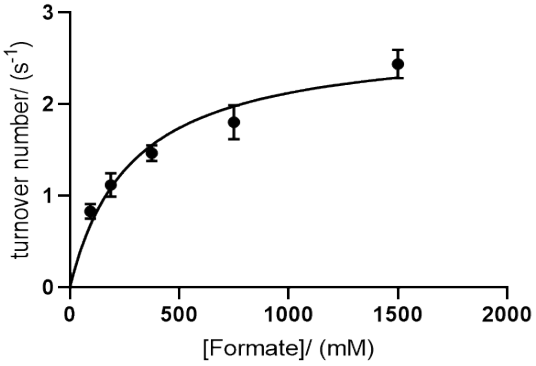

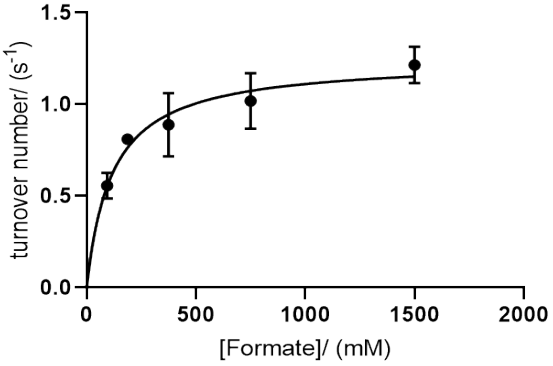

Variant GQA (A198G/ D221Q/C255A)

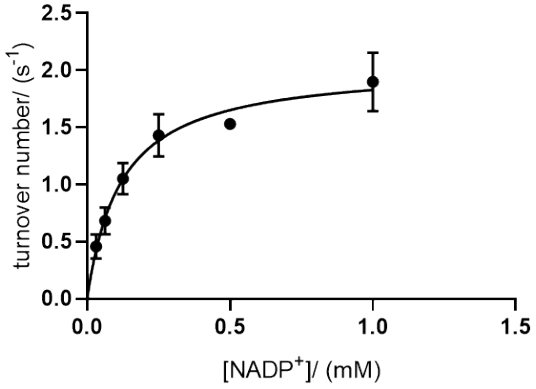

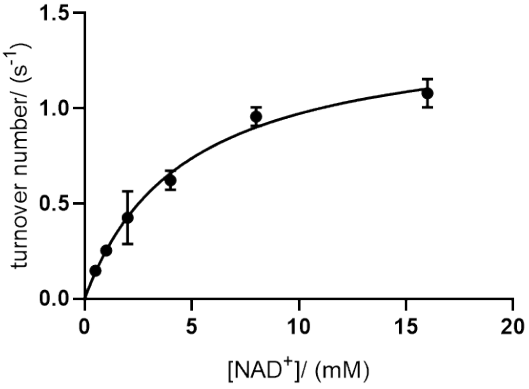

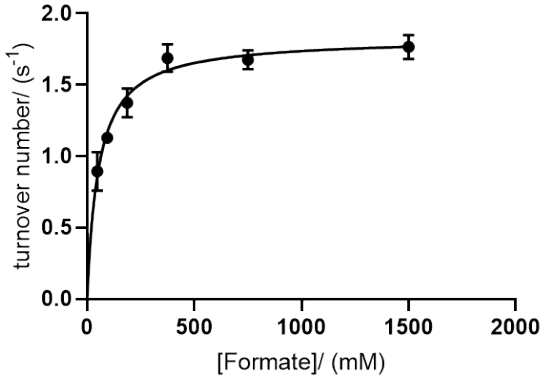

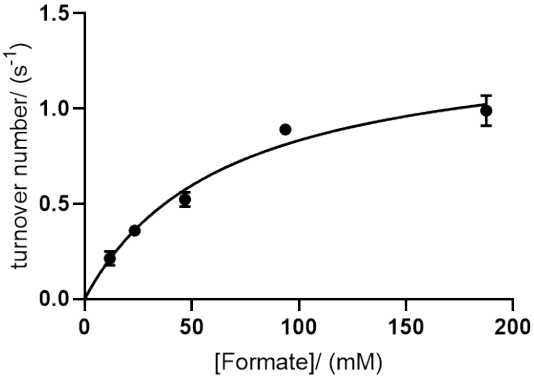

Variant GQK (A198G/ D221Q/H379K)

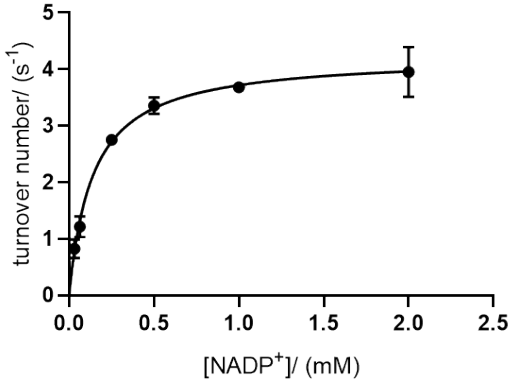

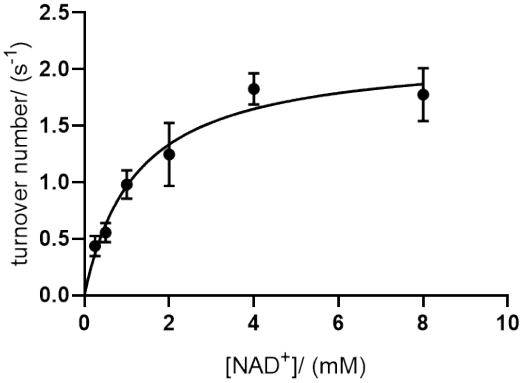

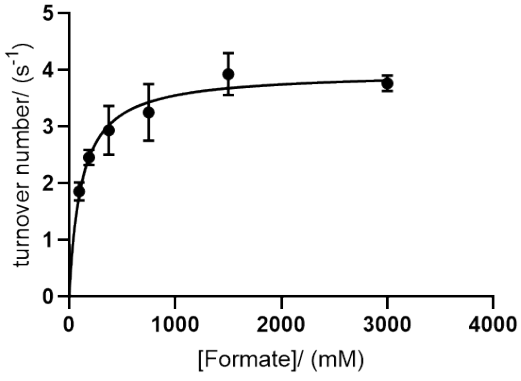

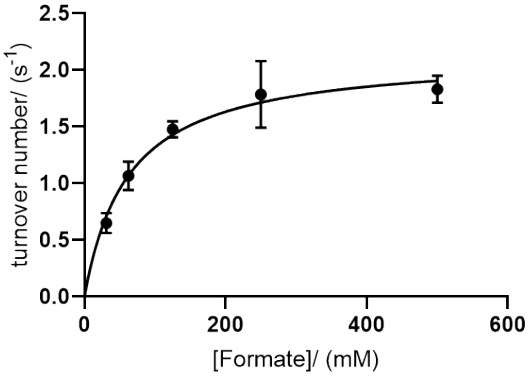

Variant GQV (A198G/ D221Q/S380V)

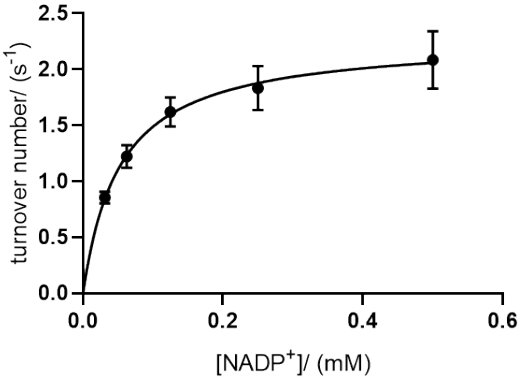

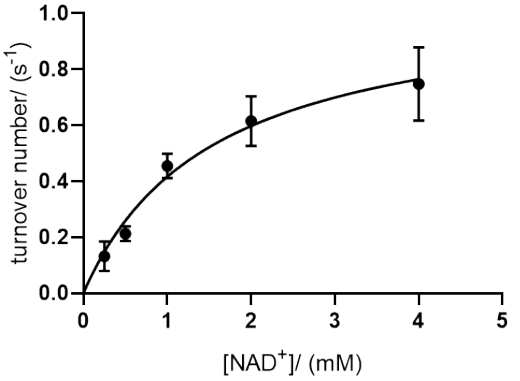

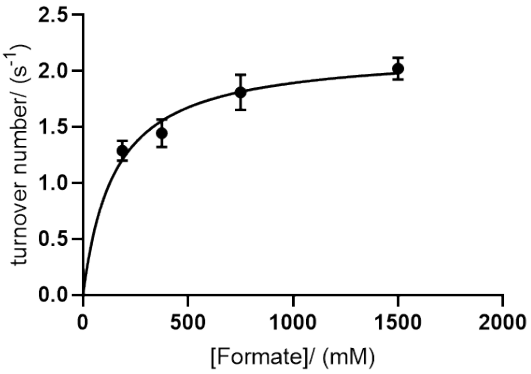

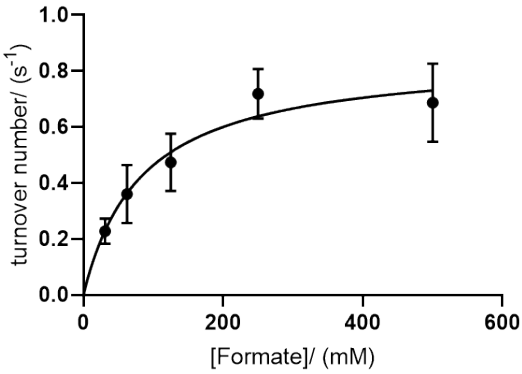

Variant GQKV (A198G/D221Q/H379K/S380V)

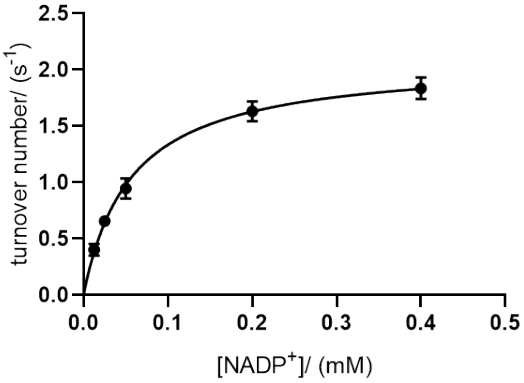

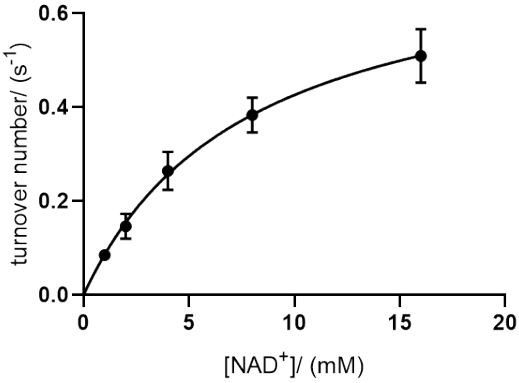

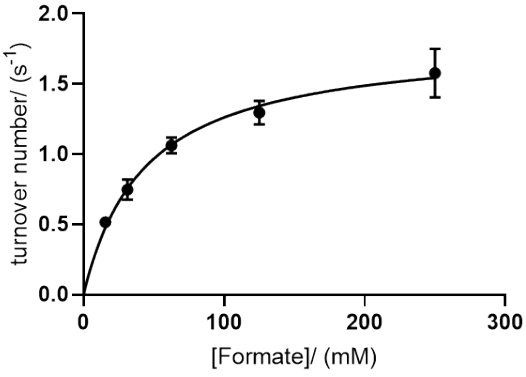

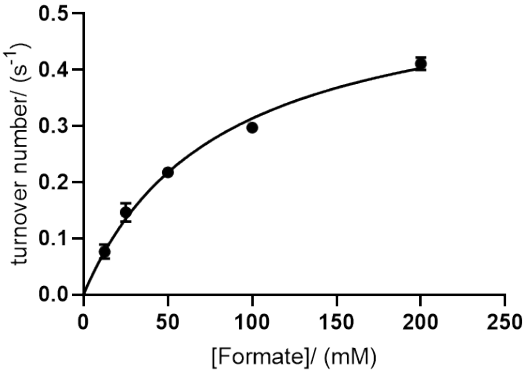

V9-GQAKC (A198G/D221Q/C255A/H379K/S380V)

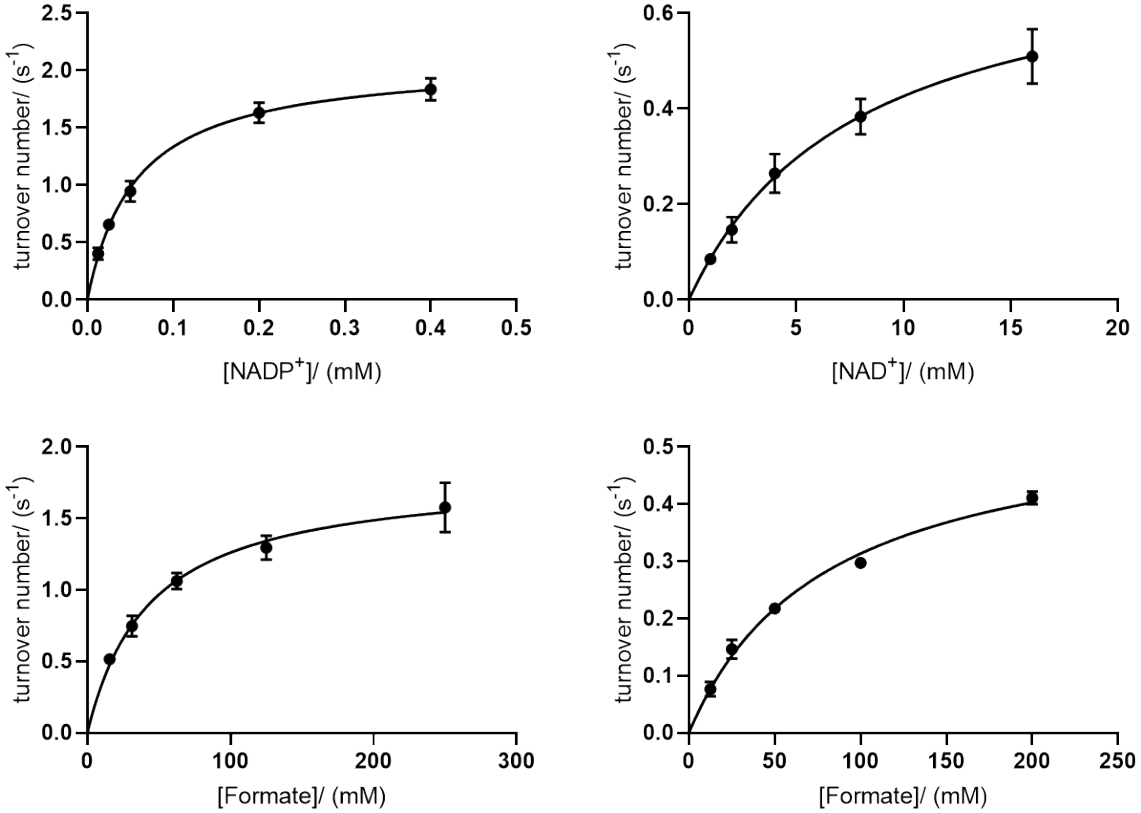

Figure S17. Michaelis Menten curves for deconvoluted PseFDH variants.

Table S1. Kinetic parameters of NADP⁺-dependent FDHs previously reported.

Variant	Substrate	K_M (mM)	k_{cat} (s^{-1})	k_{cat}/K_M ($mM^{-1}\ s^{-1}$)	CSR[c]	RCE[d,e]	Ref.
MvaFDH 3M C145S/ D221Q/ C255V	NAD^+	1.09 ± 0.04	8.22 ± 0.10	7.54	1.14	0.104	6
	Formate[a]	nd	nd	nd			
	$NADP^+$	0.92 ± 0.10	7.89 ± 1.26	8.58			
	Formate[b]	113 ± 11	nd	nd			
MvaFDH 4M C145S/ A198G/ D221Q/ C255V	NAD^+	4.10 ± 0.17	5.18 ± 0.09	1.26	16.7	0.256	6
	Formate[a]	nd	nd	nd			
	$NADP^+$	0.147 ± 0.020	3.08 ± 0.10	21.0			
	Formate[b]	98 ± 13	nd	nd			
PseFDH D221S	NAD^+	0.71 ± 45	5.0 ± 0.3	7.04	1.26	0.062	7
	Formate[a]	32 ± 2	nd	nd			
	$NADP^+$	0.19 ± 30	1.7 ± 0.2	8.9			
	Formate[b]	43	nd	nd			
PseFDH D221S/ A198G	NAD^+	0.54 ± 42	5.0 ± 0.2	9.26	0.79	0.045	7
	Formate[a]	53 ± 1	nd	nd			
	$NADP^+$	0.28 ± 25	1.8 ± 0.2	6.43			
	Formate[b]	89	nd	nd			
BstFDH WT	NAD^+	1.43	1.66	1.16	25.9	-	8
	Formate[a]	> 150	nd	nd			
	$NADP^+$	0.16	4.75	30			
	Formate[b]	55.5	nd	nd			
PseFDH D221Q/ H223N	NAD^+	1.0 ± 0.6	nd	299 ± 13	9.6	0.218	9
	Formate[a]	nd	nd	nd			
	$NADP^+$	0.35 ± 0.01	nd	31.0 ± 3.9			
	Formate[b]	63 ± 3	nd	nd			

Parameters for formate measured in the presence of (a) NAD^+ or (b) $NADP^+$. (c) Cofactor Specificity Ratio is calculated with equation $\frac{(kcat/Km)NADP-mutant}{(kcat/Km)NAD-mutant}$. (d) Relative Catalytic Efficiency is calculated with equation $\frac{(kcat/Km)NADP-mutant}{(kcat/Km)NAD-WT}$. (e) RCE values calculated with the k_{cat}/K_M values of MvaFDH WT for NAD+ (82 $mM^{-1}\ s^{-1}$) cited in Ref. [6] or of PseFDH WT for NAD^+ (142 $mM^{-1}\ s^{-1}$) reported in Ref. [7].

Table S2. Kinetics of PseFDH variants.

Variant	Substrate	K_M (mM)	k_{cat} (s^{-1})	k_{cat}/K_M ($mM^{-1}\ s^{-1}$)	CSR[c]	RCE[d,e]
WT	NAD^+	0.053 ± 0.004	7.5 ± 0.2	142.07	-	-
	Formate[a]	7.6 ± 1.1	7.8 ± 0.3	1.02		
	$NADP^+$	ND	ND	-		
	Formate[b]	ND	ND	-		
V1	NAD^+	6.4 ± 0.8	1.8 ± 0.1	0.28	93	0.183
	Formate[a]	140 ± 33	1.6 ± 0.2	0.011		
	$NADP^+$	0.127 ± 0.01	3.3 ± 0.1	26.0		
	Formate[b]	30.3 ± 0.1	2.9 ± 0.1	0.096		
V3	NAD^+	4.2 ± 0.5	1.4 ± 0.1	0.32	180	0.407
	Formate[a]	110 ± 16	1.2 ± 0.1	0.011		
	$NADP^+$	0.056 ± 0.004	3.24 ± 0.05	57.85		
	Formate[b]	31 ± 3	3.5 ± 0.1	0.11		
V7	NAD^+	8.3 ± 0.8	1.1 ± 0.1	0.13	281	0.257
	Formate[a]	162 ± 16	0.88 ± 0.2	0.005		
	$NADP^+$	0.08 ± 0.01	3.0 ± 0.1	36.62		
	Formate[b]	23 ± 3	3.1 ± 0.1	0.137		
V9	NAD^+	5.4 ± 0.7	1.5 ± 0.1	0.28	510	1.0
	Formate[a]	185 ± 34	1.64 ± 0.01	0.009		
	$NADP^+$	0.026 ± 0.001	3.69 ± 0.03	141.92		
	Formate[b]	24 ± 2.4	3.6 ± 0.1	0.16		
V13	NAD^+	9.02 ± 0.01	1.5 ± 0.1	0.17	281	0.337
	Formate[a]	89 ± 6	1.40 ± 0.03	0.016		
	$NADP^+$	0.12 ± 0.01	5.6 ± 0.1	47.90		
	Formate[b]	22 ± 2	5.6 ± 0.1	0.25		
V14	NAD^+	8 ± 1	1.09 ± 0.06	0.13	536	0.507
	Formate[a]	96 ± 14	1.16 ± 0.05	0.012		
	$NADP^+$	0.049 ± 0.006	3.6 ± 0.1	72.01		
	Formate[b]	42 ± 6	3.5 ± 0.1	0.08		
V19	NAD^+	6 ± 1	2.57 ± 0.09	0.45	71	0.226
	Formate[a]	84 ± 7	2.63 ± 0.06	0.03		
	$NADP^+$	0.13 ± 0.01	4.31 ± 0.09	32.16		
	Formate[b]	16 ± 1	4.84 ± 0.08	0.29		

Parameters for formate measured in the presence of (a) NAD^+ or (b) $NADP^+$. (c) Cofactor Specificity Ratio is calculated with equation $\frac{(kcat/Km)NADP-mutant}{(kcat/Km)NAD-mutant}$. (d) Relative Catalytic Efficiency is calculated with equation $\frac{(kcat/Km)NADP-mutant}{(kcat/Km)NAD-WT}$. (e) RCE values calculated with the k_{cat}/K_M value of PseFDH WT for NAD^+ (142 $mM^{-1}\ s^{-1}$) reported in Ref. [7].

Table S3. Kinetics of PseFDH V9 deconvoluted variants.

Variant	Substrate	K_M (mM)	k_{cat} (s^{-1})	k_{cat}/K_M (mM^{-1} s^{-1})	CSR[c]	RCE[d,e]
G (A198G)	NAD^+	0.035 ± 0.002	6.5 ± 0.1	185	-	-
	Formate[a]	8.63 ± 0.99	6.4 ± 0.2	0.74		
	$NADP^+$	ND	ND	-		
	Formate[b]	ND	ND	-		
GQ (A198G/ D221Q)	NAD^+	1.3 ± 0.4	1.2 ± 0.1	1	45	0.316
	Formate[a]	117± 27	1.24 ± 0.07	0.01		
	$NADP^+$	0.067 ± 0.009	3.0 ± 0.1	45		
	Formate[b]	281 ± 50	2.7 ± 0.2	0.009		
GQA (A198G/ D221Q/ C255A)	NAD^+	4.6 ± 0.7	1.42 ± 0.08	0.3	57	0.119
	Formate[a]	66 ± 10	1.38 ± 0.09	0.02		
	$NADP^+$	0.12 ± 0.02	2.0 ± 0.1	17		
	Formate[b]	53 ± 6	1.83 ± 0.04	0.03		
GQK (A198G/ D221Q/ H379K)	NAD^+	1.23 ± 0.25	2.16 ± 0.14	1.8	17	0.211
	Formate[a]	63 ± 11	2.15 ± 0.11	0.03		
	$NADP^+$	0.141 ± 0.015	4.2 ± 0.1	30		
	Formate[b]	116 ± 20	4.0 ± 0.1	0.03		
GQV (A198G/ D221Q/ S380V)	NAD^+	1.5 ± 0.4	1.1 ± 0.1	0.7	62	0.302
	Formate[a]	84 ± 26	0.85 ± 0.09	0.01		
	$NADP^+$	0.053 ± 0.008	2.3 ± 0.1	43		
	Formate[b]	150 ± 29	2.2 ± 0.1	0.014		
GQAV (A198G/D221Q/ C255A/S380V)	NAD^+	7.8 ± 1.4	0.76 ± 0.07	0.1	370	0.260
	Formate[a]	80 ± 7	0.56 ± 0.02	0.007		
	$NADP^+$	0.057 ± 0.004	2.09 ± 0.05	37		
	Formate[b]	44 ± 6	1.81 ± 0.08	0.04		
GQKV (A198G/D221Q/ H379K/S380V)	NAD^+	4.2 ± 0.4	1.69 ± 0.08	0.4	250	0.704
	Formate[a]	94 ± 10	1.10 ± 0.03	0.01		
	$NADP^+$	0.036 ± 0.006	3.6 ± 0.2	100		
	Formate[b]	40 ± 5	3.3 ± 0.1	0.08		
V9-GQAKC (A198G/D221Q/ C255A/H379K/ S380V)	NAD^+	5.4 ± 0.7	1.5 ± 0.1	0.3	510	1.0
	Formate[a]	185 ± 34	1.64 ± 0.01	0.009		
	$NADP^+$	0.026 ± 0.001	3.69 ± 0.03	141.92		
	Formate[b]	42 ± 6	3.5 ± 0.1	0.16		

Parameters for formate measured in the presence of (a) NAD^+ or (b) $NADP^+$. (c) Cofactor Specificity Ratio is calculated with equation $\frac{(kcat/Km)NADP-mutant}{(kcat/Km)NAD-mutant}$. (d) Relative Catalytic Efficiency is calculated with equation $\frac{(kcat/Km)NADP-mutant}{(kcat/Km)NAD-WT}$. (e) RCE values calculated with the k_{cat}/K_M value of PseFDH WT for NAD^+ (142 mM^{-1} s^{-1}) reported in Ref. [7].

Table S4. Designed oligos by DNAworks to construct the 685 bp fragment for the combinatorial library.

Name	Sequence (5' - 3')
O1	CTGGTTCGTAACTACCTGCCGTCTCACGAATGGGCTCGTAAAGGTGGTTG
O2	GCTTACGCAGTCAGCTATGTTCCAACCACCTTTACGAGCCCA
O3	GAACATAGCTGACTGCGTAAGCCACGCTTACGACCTGGAAGC
O4	CAACGGTACCAACGTGCATAGCTTCCAGGTCGTAAGCGTG
O5	TATGCACGTTGGTACCGTTGGTGCTGGTCGTATCGGTCTG
O6	CCAGACGACGCAGAACAGCCAGACCGATACGACCAGCAC
O7	GCTGTTCTGCGTCGTCTGGCTCCGTTCGACGTTCACCT
O8	**MNN**ACG**MNN**GGTGTAGTGCAGGTGAACGTCGAACGGAG
O9	GCACTACACC**NNK**CGT**NNK**CGTCTGCCGGAATCTGTTGA
O10	CCAGGTCAGGTTCAGTTCTTTTTCAACAGATTCCGGCAGACG
O11	AAAAGAACTGAACCTGACCTGGCACGCTACCCGTGAAGACAT
O12	ACGTCGCAAACCGGGTACATGTCTTCACGGGTAGCGTG
O13	GTACCCGGTTTGCGACGTTGTTACCCTGAAC**DBW**CCG
O14	TTCGGTTTCCGGGTGCAGCGGT**WVH**TTCAGGGTAACA
O15	CTGCACCCGGAAACCGAACACATGATCAACGACGAAACCC
O16	GCACCACGTTTGAACAGTTTCAGGGTTTCGTCGTTGATCATGTG
O17	TGAAACTGTTCAAACGTGGTGCTTACATCGTTAACACCGCTCG
O18	ACGGTCGCACAGTTTACCACGAGCGGTGTTAACGATGTAA
O19	TGGTAAACTGTGCGACCGTGACGCTGTTGCTCGTGCT
O20	GCCAGACGACCAGATTCCAGAGCACGAGCAACAGCGTC
O21	CTGGAATCTGGTCGTCTGGCTGGTTATGCGGGTGACGTG
O22	CCGGCTGGGGGAACCACACGTCACCCGCATAACCA
O23	TGGTTCCCCCAGCCGGCTCCGAAAGACCACCCGTG
O24	GTTGTACGGCATGGTACGCCACGGGTGGTCTTTCGGAG
O25	GCGTACCATGCCGTACAACGGTATGACCCCGCACATCTC
O26	GCGGTCAGGGTGGTACCAGAGATGTGCGGGGTCATACC
O27	TGGTACCACCCTGACCGCTCAGGCTCGTTACGCTGC
O28	CCAGGATTTCACGGGTACCAGCAGCGTAACGAGCCTGA
O29	TGGTACCCGTGAAATCCTGGAATGCTTCTTCGAAGGTCGTCC
O30	GATCAGGTATTCGTCACGGATCGGACGACCTTCGAAGAAGCATT
O31	GATCCGTGACGAATACCTGATCGTTCAGGGTGGTGCTCTGG
O32	**AVYMNN**AGCACCGGTACCAGCCAGAGCACCACCCTGAAC
O33	CTGGTACCGGTGCT**NNKRBT**TACTCTAAAGGTAACGCTACCGG
O34	AATTTAGCAGCTTCTTCAGAACCACCGGTAGCGTTACCTTTAGAGTAA
O35	TGGTTCTGAAGAAGCTGCTAAATTCAAAAAAGCTGTTTAAGCTAGCGC
O36	GTCGACATACTCGAGCGGCCGCGCTAGCTTAAACAGCTTTTTTG

For oligos 8, 9, 13, 14, 32 and 33 the original bases provided by the server were exchanged by degenerate codons NNK/MNN, DBW/WVH or RBT/AVY.

Table S5. Oligos designed for PseFDH specific mutations.

Name	Sequence (5' - 3')
A198G_Fw	GCTATGCACGTTGGTACCGTT**GGT**GCTGGTCGT
A198G_Rv	CAGACCGATACGACCAGCACCAA**CGG**TACC
D221Q_Fw	CTGCACTACACCCAGCGTCACC**GTC**TGCCG
D221Q_Rv	ACGGTGACG**CTG**GGTGTAGTGCAGGTGAACGTC
C255A_Fw	GTTGTTACCCTGAAC**GCA**CCGCTGCACCCG
C255A_Rv	GTGCAGCGGTG**CGT**TCAGGGTAACAACGTC
H379K_Fw	GTACCGGTGCT**AAG**TCTTACTCTAAAGGTAAC
H379K_Rv	GCGTTACCTTTAGAGTCT**ACC**TTAGCACCGGT
H379K/S380V_Fw	GTACCGGTGCT**AAGGTT**TACTCTAAAGGTAAC
H379K/S380V_Rv	GCGTTACCTTTAGAG**TAAACC**TTAGCACCGGT

The underlined and bold bases represent the codons modified for specific mutations.

2. Protocols

Computational models

The computational models used in this study were built using the apo state X-ray crystal structure (Protein Data Bank (PDB) accession number 2GO1) and the holo state X-ray crystal structure (PDB accession number 2GUG crystallized in the presence of formate in the active site) as a starting point to run MD simulations:

- 2GO1: NAD-dependent formate dehydrogenase from *Pseudomonas sp. 101* (APO form). (2.10 Å resolution).
- 2GUG: NAD-dependent formate dehydrogenase from Pseudomonas sp.101 in complex with formate; *Pseudomonas sp. 101* (holo, formate is present, cofactor is not). (2.28 Å resolution)

In these X-Ray structures, the region near the cofactor (residues 257-262) and the loop C-terminus (375-400) was unsolved. These unsolved regions in 2GUG were reconstructed using 2NAD as the reference structure of structure, and a complete PseFDH model (400 residue length) was built as described in the Methods section of the manuscript. NAD^+ and $NADP^+$ cofactors were placed in the active site of holo (presence of formate) PDB 2GUG by structural alignment with PDB 2NAD (that contains NAD^+ cofactor).

- 2NAD: HIGH RESOLUTION STRUCTURES OF HOLO AND APO FORMATE DEHYDROGENASE, presence of NAD cofactor and azide ion; *Pseudomonas sp. 101.* (2.05 Å resolution)

The structure used as a reference (2NAD) was crystallized in the ternary complex (FDH-NAD^+-azide), which can be considered as an analog of the transition state in the closed conformation [3], this can be confirmed by RMSD value (shown in Figure S14.b and c). Related FDH with solved structure available from the PDB Bank:

- 2GSD[5]: NAD-dependent formate dehydrogenase from bacterium *Moraxella sp.* C2 in complex with NAD and azide. (1-399 residues, 1.95 Å resolution).

As shown in Figure S15 and the computed RMSD values, the reconstructed regions (Figure S15.b, shown in orange) adopt a similar conformation that in the holo-MorFDH structure. The extra 7 residues in the C-terminal region present in the computational model that were built with homology modeling tools are shown in Figure S15.c (393-400, shown in orange). By comparing the structure of holo-MorFDH (PDB:2GSD) with the starting point for MD simulations (shown in green in Figure S15), it can be seen that the additional residues built in the model are in a very similar conformation than in the holo-MorFDH structure 2GSD. The latter structure is described to be in a closed conformation due to the presence of the cofactor and azide. The small RMSD (0.281 Å) obtained when comparing 2GSD structure and the generated computational model is indicating that the model correctly describes the major closed conformation of the holo-protein system and is thus a good starting point for running the MD simulations.

QuikChange protocol

Reaction mix

H_2O	add to 50 µl	
5X Phusion GC buffer	10 µl	
10 mM dNTPs	1 µl	
Forward primer	2.5 µl	
Reverse primer	2.5 µl	
Template DNA		50 ng (1-10 µl)
Phusion DNA Polymerase	0.5 µl	
Final volume	50 µl	

PCR Programm

Cycle step	Temperature	Time	Cycles
Initial Denaturation	98 ºC	30 s	1
Denaturation	98 ºC	10 s	30
Annealing	55 / 60 ºC	30 s	30
Extension	72 ºC	2 min (15-30s/kb)	30
Final Extension	72 ºC	10 min	1
	4 ºC	hold	1

1.- Run 5 µl of the PCR product and the negative control (see a band around 4.5 kbp and no band for the negative control).
2.- Add 1µl of DpnI restriction enzyme to the PCR product, incubate at 37 ºC overnight.
3.- Purify PCR product

ADO fragment synthesis

1.- Dilute each primer to 10 µM in water
2.- In a new tube, mix 1µl of each primer

First ADO step: Without flanking primers.

Reaction Mix:

4 µl of the equimolar mixture
5 µl r of buffer High GC (phusion kit) it has $MgCl_2$
5 µl of 2mM dNTPs
1 µl of Phusion polymerase
35 µl ddH_2O
50 µl Final volume

PCR Program:

Cycle step	Temperature (°C)	Time	Cycles
Denaturation	95ºC	20s	20
Annealing	50ºC	30s	
Extension	70°C	1min	
Hold	4ºC		

Second ADO step: With flanking primers.

Reaction Mix:

1 µl of resulting assembly reaction
5 µl of buffer High GC (phusion kit) it has $MgCl_2$
5 µl of 2mM dNTPs
1 µl Primer 1
1 µl Primer 36
1 µl of Phusion polymerase
36 µl ddH_2O
50 µl Final volume

PCR Program:

Cycle step	**Temperature (°C)**	**Time**	**Cycles**
Initial Denaturation	95	2 min	1
Denaturation	95	20 s	25
Annealing	50	30 s	
Extension	70	1 min	
Final extension	70	5 min	1
Hold	4		

3. References

(1) Filippova, E. V.; Polyakov, K. M.; Tikhonova, T. V.; Stekhanova, T. N.; Boĭko, K. M.; Popov, V. O. Structure of a New Crystal Modification of the Bacterial NAD-Dependent Formate Dehydrogenase with a Resolution of 2.1 Å. *Crystallogr. Rep.* **2005**, *50*, 796-800. https://doi.org/10.1134/1.2049398.

(2) Filippova, E. V.; Polyakov, K. M.; Tikhonova, T. V.; Stekhanova, T. N.; Boiko, K. M.; Sadykhov, I. G.; Tishkov, V. I.; Popov, V. O.; Labru, N. Crystal Structures of Complexes of NAD+-Dependent Formate Dehydrogenase from Methylotrophic Bacterium Pseudomonas Sp. 101 with Formate. *Crystallogr. Rep.* **2006**, *51*, 627-631. https://doi.org/10.1134/S1063774506040146.

(3) Lamzin, V. S.; Dauter, Z.; Popov, V. O.; Harutyunyan, E. H.; Wilson, K. S. High Resolution Structures of Holo and Apo Formate Dehydrogenase. *J Mol Biol*. **1994**, *263 (3)*, 759–785. https://doi.org/10.1006/jmbi.1994.1188.

(4) K. B. Cahn, J.; A. Werlang, C.; Baumschlager, A.; Brinkmann-Chen, S.; L. Mayo, S.; H. Arnold, F. A General Tool for Engineering the NAD/NADP Cofactor Preference of Oxidoreductases. *ACS Synth. Biol.* **2016**, *6* (2), 326–333. https://doi.org/10.1021/acssynbio.6b00188.

(5) Shabalin, I. G.; Filippova, E. V.; Polyakov, K. M.; Sadykhov, E. G.; Safonova, T. N.; Tikhonova, T. V.; Tishkov, V. I.; Popov, V. O. Structures of the Apo and Holo Forms of Formate Dehydrogenase from the Bacterium Moraxella Sp. C-1: Towards Understanding the Mechanism of the Closure of the Interdomain Cleft. *Acta Crystallogr D Biol Crystallogr.* **2009**, *65*, 1315-1325. https://doi.org/10.1107/S0907444909040773.

(6) Hoelsch, K.; Sührer, I.; Heusel, M.; Weuster-botz, D. Engineering of Formate Dehydrogenase : Synergistic Effect of Mutations Affecting Cofactor Specificity and Chemical Stability. *App Microbial Biotechnol.* **2013**, *97 (6)*, 2473–2481. https://doi.org/10.1007/s00253-012-4142-9.

(7) Alekseeva, A. A.; Fedorchuk, V. V.; Zarubina, S. A.; Sadykhov, E. G.; Matorin, A. D.; Savin, S. S.; Tishkov, V. I. The Role of Ala198 in the Stability and Coenzyme Specificity of Bacterial Formate Dehydrogenases. *Acta Naturae* **2015**, *7 (1)*, 60-69. https://doi.org/10.32607/20758251-2015-7-1-60-69.

(8) Hatrongjit, R.; Packdibamrung, K. Enzyme and Microbial Technology A Novel NADP+-Dependent Formate Dehydrogenase from Burkholderia Stabilis 15516 : Screening , Purification and Characterization. *Enzyme Microb. Technol.* **2010**, *46* (7), 557–561. https://doi.org/10.1016/j.enzmictec.2010.03.002.

(9) Ihara, M.; Kawano, Y.; Urano, M.; Okabe, A. Light Driven CO_2 Fixation by Using Cyanobacterial Photosystem I and NADPH-Dependent Formate Dehydrogenase. **2013**, *8* (8), 1–8. https://doi.org/10.1371/journal.pone.0071581.